Tunable Surface Plasmon Dynamics

By

Ernesto Alexander Ramos

Submitted to the Department of Electrical Engineering and Computer Science and the Graduate Faculty of the University of Kansas in partial fulfillment of the requirements for the degree of Master of Science.

Dr. Alessandro Salandrino, Chair

Dr. Christopher Allen

Dr. Rongqing Hui

Date Defended: 10 May 2019

The thesis committee for E. A. Ramos certifies that this is the approved version of the following thesis:

Tunable Surface Plasmon Dynamics

Chair: Dr. Alessandro Salandrino

Co-Chair: Dr. Christopher Allen

Co-Chair: Dr. Rongqing Hui

Date Approved: 10 May 2019

Abstract

Due to their extreme spatial confinement, surface plasmon resonances show great potential in the design of future devices that would blur the boundaries between electronics and optics. Traditionally, plasmonic interactions are induced with geometries involving noble metals and dielectrics. However, accessing these plasmonic modes requires delicate election of material parameters with little margin for error, controllability, or room for signal bandwidth. To rectify this, two novel plasmonic mechanisms with a high degree of control are explored:

For the near infrared region, transparent conductive oxides (TCOs) exhibit tunability not only in "static" plasmon generation (through material doping) but could also allow modulation on a plasmon carrier through external bias induced switching. These effects rely on the electron accumulation layer that is created at the interface between an insulator and a doped oxide. Here a rigorous study of the electromagnetic characteristics of these electron accumulation layers is presented. As a consequence of the spatially graded permittivity profiles of these systems it will be shown that these systems display unique properties. The concept of Accumulation-layer Surface Plasmons (ASP) is introduced and the conditions for the existence or for the suppression of surface-wave eigenmodes are analyzed.

A second method could allow access to modes of arbitrarily high order. Sub-wavelength plasmonic nanoparticles can support an infinite discrete set of orthogonal localized surface plasmon modes, however only the lowest order resonances can be effectively excited by incident light alone. By allowing the background medium to vary in time, novel localized surface plasmon dynamics emerge. In particular, we show that these temporal permittivity variations lift

the orthogonality of the localized surface plasmon modes and introduce coupling among different angular momentum states. Exploiting these dynamics, surface plasmon amplification of high order resonances can be achieved under the action of a spatially uniform optical pump of appropriate frequency.

Acknowledgements

This work was supported in part by the Air Force Office of Scientific Research (AFOSR) under the grant FA9550-16-1-0152.

Table of Contents

TABLE OF FIGURES ..... **VII**

CHAPTER 1. INTRODUCTION **1**

CHAPTER 2. BACKGROUND **4**

PLASMONICS: THE DIELECTRIC FUNCTION 4
PLASMONICS: CONDUCTIVITY 6
PLASMONICS: THE DRUDE THEORY OF METALS 7
PLASMONICS: THE SURFACE PLASMON POLARITON 10
THE MOS CAPACITOR 13
ELECTRO-OPTICAL MODULATORS 16

CHAPTER 3. THE ACCUMULATION SURFACE PLASMON **20**

TRANSPARENT CONDUCTIVE OXIDES 20
THE THIN FILM SPP 21
VIRTUAL THIN FILMS AND THE ASP 22
ANALYSIS AND SIMULATED RESULTS 23

CHAPTER 4. PARAMETRIC PLASMONIC RESONANCE **33**

PARAMETRIC RESONANCE 33
MULTIPOLAR MODES 35
POLARIZATION DENSITY IN A PLASMONIC NANOPARTICLE 40
BACKGROUND PERMITTIVITY MODULATION 43

CHAPTER 5. CONCLUSIONS AND FUTURE WORK **48**

CHAPTER 6. REFERENCES **51**

Table of Figures

Figure 2.1: Notional plot of the real part of a metal's dielectric function with ω_p = 10 THz 10
Figure 2.2: Distinct infinite half spaces with a TM Mode Propagating on the Interface 11
Figure 2.3: Notional Architecture of an ITO MOS Capacitor 14
Figure 3.1: Imaginary parts of dielectric function of a) gold and b) various TCO films deposited using pulsed laser deposition. [13] 21
Figure 3.2: a) SPP model, b) Thin Film SPP Model, c) Dispersion relation for antisymmetric (a) and symmetric (s) modes of a thin-film SPP [15] 22
Figure 3.3: Electrostatic potential and charge density as a function of position in a Silicon-dioxide/ITO MOS structure. The ITO doping concentration is $N_d = 10^{25}\ m^{-3}$ and the applied bias is 1 V. 23
Figure 3.4: Permittivity profile in the accumulation layer in an ITO film with three different doping concentrations. 25
Figure 3.5: (a) Magnetic Field Profile and (b) β of an ASP in a SiO2–ITO MOS structure with doping concentration $N_d = 10^{27}[m^{-3}]$ and surface potential $\Phi_S = 3\Phi_T$ 29
Figure 3.6: Normalized Propagation Constant and propagation length of the ASP in a SiO2–ITO MOS structure 30
Figure 4.1: Time Varying RLC circuit 34
Figure 4.2: a) Spectral distributions of the resonant modes of a plasmonic nanosphere. b) Surface polarization charge density for the first few modes of a plasmonic nanosphere. 37
Figure 4.3: Interaction of various incident spherical harmonics with a subwavelength particle 38
Figure 4.4: Scattering from a spherical particle partitioned by angular momentum order 39
Figure 4.5: Temporal evolution of the potential and polarization currents of the octupolar mode of a plasmonic nanosphere 42
Figure 4.6: Phase-space trajectory of an attenuated eigenmode 43
Figure 4.7: a) Temporal evolution of the stored energy in the octupolar mode of a plasmonic nanosphere when the background permittivity modulation depth has been exceeded and b) total energy dynamics as a function of modulation depth 45
Figure 4.8: Schematic representation of one full-modulation cycle, leading to parametric regeneration of the plasmonic eigenmode 46

Chapter 1. Introduction

Today's electronics engineers and product designers face two facts: consumers demand smaller products and their appetite for data is seemingly insatiable. This continued drive towards miniaturization has been coupled with increasing bandwidth and latency requirements pushing electronics to their hard, physical limits. Meanwhile, the optical regime has flourished: large investments by the telecommunications industry and maturity in fiber technology has opened THz of bandwidth in the 1550 nm range [1]. Effective means of coupling electronic modes to optical modes do exist, but these Electro-optic modulators (EOM) are relatively large and have form factors that are not amenable to integration with small electronic devices [2], [3]. If efficient and tunable EOM devices could be made *small* enough, then concepts like optical computing could be realized and electro-optical chips could make their way into consumer level devices.

Plasmonics is a natural space to search for potential EOM device architectures. The plasmon, defined as the quanta of a coupled mode between an electromagnetic wave (a photon) and a loosely bound electron gas (bulk metal plasma) has many desirable characteristics. Not only does it lie at this desirable intersection between electrons and photons, but in the case of the Surface Plasmon Polariton (SPP), the spatial confinement of the mode can be very tight; suggesting a potential for very small devices. Additionally, this confinement can generate local electric field strengths of large magnitude, enhancing non-linear responses in the surrounding materials.

Surface plasmon-polaritons (SPP) have been well understood for over 50 years, however their use in practical and realizable photonic devices has been limited. This work aims to explore novel plasmonic architectures and their associated phenomenology. The two architectures

presented have been carefully chosen: not only for their potential as parts of photonic devices but also for their mathematical tractability.

The architecture's potential as a device pivots around the availability of either controllable modal selectivity, or a modulation abstraction of some kind. Modal selectivity lends itself to sensor design, since the presence of a signal would imply some phenomenon of interest has occurred to trigger the designed mode, thereby this phenomenon has become observable. From an engineering perspective, a simple propagating oscillation is not very useful without being able to attach or extract information from it. As such, for an architecture to be useful in a communications setting, some mathematical abstraction of signal modulation (be it intensity, phase or polarization modulation) must be realizable.

Surface plasmon resonances in transparent conductive oxides (TCOs) and suspended noble metal nanoparticles will be shown to be, by our definition, *useful* devices. The TCO architecture will be inspired by the metal-oxide semiconductor (MOS), where tunability is provided by material doping and a variable applied electric bias. This tunability acts as both a method of device calibration and, potentially, signal modulation.

The noble metal nanoparticle architecture will consist of gold particles in a colloidal suspension with organic molecules; tunability is provided by spatially uniform temporal modulation of the background permittivity. As will be shown, given a design spatial pump, the system's response is highly selective and local fields are highly nonlinear. Such a device could make a discerning sensor. But, from a light-matter interaction perspective, the device could also be used to study novel physics of high powers of χ (electric susceptibility) on geometric scales smaller than the wavelength.

The exploration of each of these regimes is two-fold; with both an analytical and a numerical treatment. The regimes are mathematically tractable since, in the strictest sense, no new theory is introduced or required for a faithful representation of the physics. Instead, classic analytic methods are applied and verified numerically. The agreement between these treatments should lead to workable models for the phenomenology involved and these models should serve as a starting point for the future engineering of *useful* plasmonic devices.

Chapter 2. Background

Plasmonics: The Dielectric Function

The interactions between light and metals are manifold and are not generally treated as one discrete phenomenon. The quantum mechanical nature of light leads to highly distinct phenomenological regimes depending on the wavelength of the incident light and the atomic as well as crystallographic properties of the bulk metal the light interacts with. This is best exemplified by the superficially similar Photoelectric and Photovoltaic effects. Although, in both cases photons elevate charge carriers to a higher energy state, the results are vastly different: in the Photoelectric effect ballistic conduction radiates a photon while in the Photovoltaic [4] effect diffusive conduction generates an electromotive force.

The study of Plasmonics alleviates these quantum mechanical considerations by taking a *macroscopic* approach. Rather than finding the point-by-point properties of some interaction, the underlying physics is analyzed in a *modal* sense. This effective averaging of the *micro* phenomena allows for the use of Maxwell's equations and the classical Drude model as the analytic tools. Equation set (2.1) is the differential ("local"), macroscopic form of classical Maxwell's equations where **E** and **H** represent the electric and magnetic vector field quantities, **D** and **B** the electric displacement and magnetic flux density, **J** the free current density and ρ the free charge density.

$$\begin{aligned} \nabla \cdot \mathbf{D} &= \rho \\ \nabla \cdot \mathbf{B} &= 0 \\ \nabla \times \mathbf{E} &= -\frac{\partial \mathbf{B}}{\partial t} \\ \nabla \times \mathbf{H} &= \mathbf{J} + \frac{\partial \mathbf{D}}{\partial t} \end{aligned} \tag{2.1}$$

Outside of a vacuum these equations are an insufficient model since real materials contain bound charges. This is corrected with the auxiliary fields:

$$\mathbf{D} = \epsilon_0 \mathbf{E} + \mathbf{P} \tag{2.2}$$

$$\mathbf{H} = \frac{1}{\mu_0} \mathbf{B} + \mathbf{M} \tag{2.3}$$

where **P** and **M** are the polarization and magnetization fields and ϵ_0 and μ_0 are the free space permittivity and permeability.

It is standard to assume linearity, non-magnetism and isotropy. This means any charge displacement is "inline" with the electric field; expressed mathematically as

$$\mathbf{P} = \epsilon_0 \chi_e \mathbf{E} \tag{2.4}$$

where χ_e is the electric susceptibility to polarization. It is clear to see:

$$\mathbf{D} = \epsilon_0 \left(1 + \chi_e\right) \mathbf{E} = \epsilon_0 \epsilon \mathbf{E} \tag{2.5}$$

where ϵ is the material dielectric. In general, this dielectric function is a function of position, direction and time and can be further generalized by considering only the time harmonic response. Assuming the stimulus field is of the form $\mathbf{E}(t) = \mathbf{A} e^{-i\omega t}$ and in the limit $t \to \infty$, we cast the problem in the Fourier domain:

$$\mathbf{D}(\omega) = \epsilon_0 \epsilon(\omega) \mathbf{E}(\omega) \tag{2.6}$$

At this stage $\epsilon(\omega)$ neatly encompasses all subwavelength material characteristics into one, concise, effective permittivity function. The determination of and physical understanding of this function is central to the modal analysis that comprises this work.

Plasmonics: Conductivity

To further expound on the dielectric function as it relates to plasmonics, and to gain intuition, it is useful to tie it to the standard engineering quantity which defines a metal: conductivity. Equation (2.4) established that a field displaces charge. A current density is defined as a charge density times a velocity, which is the time derivative of a displacement. Thus:

$$\mathbf{J} = \frac{\partial \mathbf{P}}{\partial t} \tag{2.7}$$

In a linear, isotropic metal, internal currents follow the field:

$$\mathbf{J} = \sigma \mathbf{E} \tag{2.8}$$

where σ is the conductivity of the metal.

Equating (2.7) and (2.8), taking the time harmonic time derivative of (2.7) and substituting (2.4):

$$\sigma(\omega) = -i\omega\epsilon_0\chi_e(\omega) \tag{2.9}$$

Solving for χ_e and plugging back into (2.5),

$$\mathbf{D}(\omega) = \epsilon_0\left(1 + \frac{i\sigma(\omega)}{\epsilon_0\omega}\right)\mathbf{E}(\omega) \tag{2.10}$$

establishing that $\epsilon(\omega) = \left(1 + i\sigma(\omega)/\epsilon_0\omega\right)$. From here, it should be clear that this is a complex function and any absorptive loss in the system, nominally attributed to $\epsilon_i(\omega) = \mathrm{Im}\left\{\epsilon(\omega)\right\}$ is a direct function of the real part of the conductivity. The imaginary part of the conductivity will thereby determine *how* polarizable the metal is [5], [6].

Plasmonics: The Drude Theory of Metals

Plasmons are the quanta of a propagating plasma oscillation and this can be directly linked to conductivity. In a metal, electrons are weakly bound to their originating atoms and, within certain frequency limits, can be modeled as an ideal electron gas; a plasma in which collision interactions with the crystal lattice are ignored. For the purposes of this work, the Drude model for electron collisions [5] of the plasma will be employed to attain the metal's dielectric function.

The velocity of any particular electron in a field as a function of time is as follows:

$$\mathbf{v}_{elec} = \mathbf{v}_0 - \frac{q\mathbf{E}t}{m} \tag{2.11}$$

where m is the mass of the electron and $\mathbf{v}_0$ is the velocity immediately after a collision and q is the fundamental charge of an electron. If it is assumed that $\mathbf{v}_0$ (the direction an electron is scattered) is random after a collision, then taking the average:

$$\mathbf{v}_{avg} = \frac{-q\tau\mathbf{E}}{m} \tag{2.12}$$

where τ must be the average time before a collision, this is commonly referred to as the relaxation time and its inverse $1/\tau = \gamma$ is the collision frequency.

With some substitutions into (2.8) and keeping units consistent, a relation with conductivity can be derived.

$$\mathbf{J} = \frac{q^2 n\tau}{m}\mathbf{E} \rightarrow \sigma = \frac{q^2 n\tau}{m} \tag{2.13}$$

Thus, the collision frequency for a metal is

$$\gamma = \frac{q^2 n}{\sigma m} \tag{2.14}$$

It should be noted that the conductivity may be a function of frequency and any crystal effects can be built into *m* as an effective mass.

Now, an electron displaced from its equilibrium position by *x* induces a net dipole of δ=-*qx*. Similarly, for a set of *n* electrons with displacement **x**, the total polarization will be **P = -*nq*x.**

If **x** is a displacement driven by an oscillating electric field and there exists no restoring force since the electrons are unbound, the following equation for a driven harmonic oscillator applies:

$$m\frac{d^2\mathbf{x}(t)}{dt^2} + \gamma m\frac{d\mathbf{x}(t)}{dt} + 0 = -q\mathbf{E}(t) \tag{2.15}$$

If the driving field **E***(t)* is a complex sinusoid, then the response **x***(t)* will behave as some delayed (phase-shifted) version of the stimulus and a solution could be $\mathbf{x}(t) = \mathbf{B}e^{-i\omega t}$. Plugging back into (2.15) and solving for **B**:

$$\mathbf{x}(t) = \left(\frac{q}{m\omega(i\gamma + \omega)}\right)\mathbf{A}e^{-i\omega t} = \left(\frac{q}{m\omega(i\gamma + \omega)}\right)\mathbf{E}(t) \tag{2.16}$$

this response induces the polarization:

$$\mathbf{P} = \left(\frac{-nq^2}{m\omega(i\gamma + \omega)}\right)\mathbf{E}(t) \tag{2.17}$$

Applying the analysis of the previous section: taking the derivative of **P** and equating it to (2.8), an effective free charge conductivity is found:

$$\sigma(\omega) = \frac{inq^2}{m(i\gamma + \omega)} \tag{2.18}$$

Inspecting (2.10), the dielectric function for a "perfect" Drude metal with no interband transitions is extracted

$$\epsilon(\omega) = 1 - \frac{nq^2}{m\epsilon_0\left(\mathrm{i}\gamma\omega + \omega^2\right)} \tag{2.19}$$

Defining $\omega_p{}^2 = nq^2 / m\epsilon_0$ as the plasma frequency of a metal is particularly useful, since it acts like a frequency cutoff for all transverse plasmonic modes. Figure 2.1 illustrates that below the plasma frequency the real part of the permittivity is negative and the material is "metallic". That is, EM wave propagation in this regime is forbidden (In standard electromagnetics literature, this is true of all metals assumed to be PEC). Above ω_p, the permittivity is positive, and well beyond ω_p, the real part approaches 1; this dominates the total dielectric function and the imaginary part must approach zero. Electrons have mass; therefore they will lag behind "faster" excitations, denoted by a more imaginary conductivity as frequency increases. Effectively, at sufficiently high frequencies ideal electron gasses become transparent, and the only modes available are in the transverse direction, with the dispersion becoming "light-like" [7].

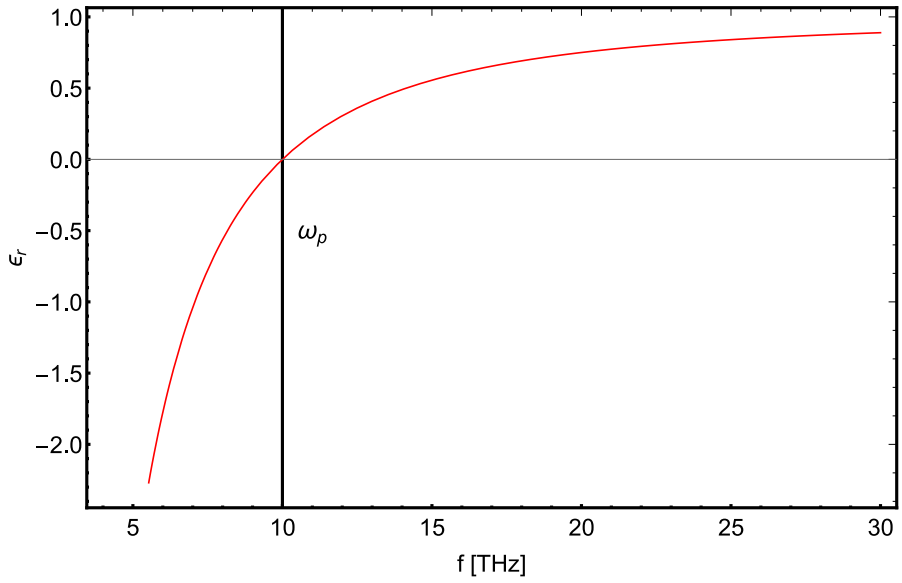

Figure 2.1: Notional plot of the real part of a metal's dielectric function with ω_p = 10 THz

Plasmonics: The Surface Plasmon Polariton

The previous section explained the mechanics of a plasma oscillation but did not describe a method to couple to it using light. It should be intuitive that any two modes with matching frequencies and wavevectors can interact freely with each other since momentum is conserved. If this match is observed between a free photon in some medium and a transverse plasmon mode in some metal, the resultant resonance is termed a Surface Plasmon Polariton (SPP) [7], [8]. As will be shown, achieving this match is particularly feasible at the interface of a dielectric and a metal and the field will be evanescent on either side of the interface.

Starting with two infinite half spaces, as shown in Figure 2.2, each with a respective dielectric ϵ_1 or ϵ_2, and defining the interface at $x=0$, the characteristics of a TM mode propagating in the positive y direction will be found. The fundamental fields in each half space must satisfy the following boundary conditions:

$$E_{1z} = E_{2z}$$
$$H_{1y} = H_{2y} \tag{2.20}$$
$$D_{1x} = D_{2x} \rightarrow \epsilon_1 E_{1x} = \epsilon_2 E_{2x}$$

, noting that the TM mode will contain an **H** field component only in the *y* direction and the normal component of the displacement field **D** must be conserved.

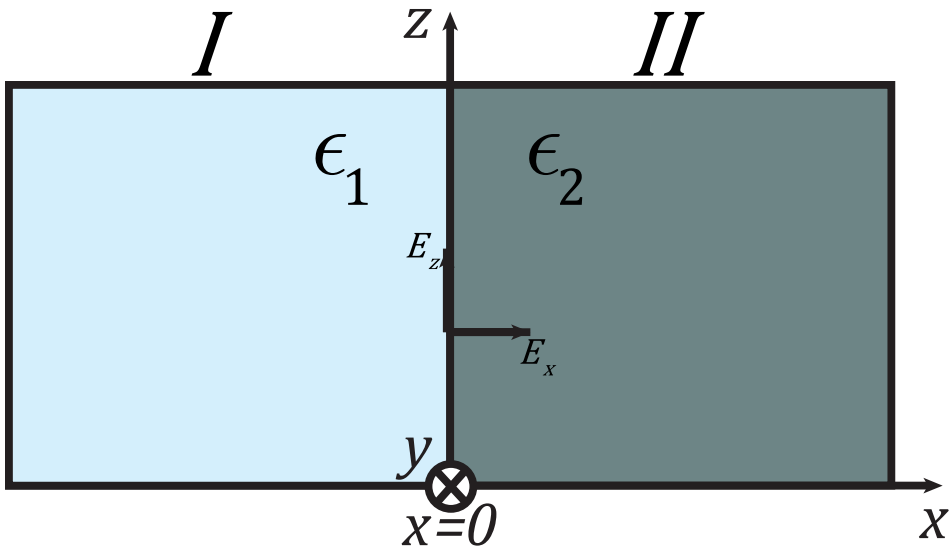

Figure 2.2: Distinct infinite half spaces with a TM Mode Propagating on the Interface

Assuming no currents, and modifying (2.1) by normalizing $\mathbf{H}$ as $\mathbf{H} = -i\sqrt{\mu_0 / \epsilon_0}\tilde{\mathbf{H}}$ [9] and considering only the components relevant to a TM mode; the spatial Maxwell's equations reduce to:

$$\begin{array}{cc} I & II \\ -\frac{\partial H_{1y}}{\partial z} = k_0 \epsilon_1 E_{1x} & -\frac{\partial H_{2y}}{\partial z} = k_0 \epsilon_2 E_{2x} \\ \frac{\partial H_{1y}}{\partial x} = k_0 \epsilon_1 E_{1z} & \frac{\partial H_{2y}}{\partial x} = k_0 \epsilon_2 E_{2z} \end{array} \tag{2.21}$$

where $k_0 = \frac{\omega}{c}$ is the wave number and the fields are partitioned into their respective spaces *I* and *II*. Recognizing that $\frac{\partial H_{1y}}{\partial z} = k_{1z}$ and $\frac{\partial H_{1y}}{\partial x} = -k_{1x}$, where k_{Nr} is the spatial frequency of the propagation in the *N*th space in the *r* component and recognizing that the waves propagating outwards from the interface along *x* into the spaces have opposite signs ($\mathrm{Sgn}(k_{1x}) = -\mathrm{Sgn}(k_{2x})$), the following can be found:

$$\begin{aligned} I \quad & k_{1x} H_{1y} = -\epsilon_1 k_0 E_{1x} \\ II \quad & k_{2x} H_{2y} = \epsilon_2 k_0 E_{2x} \end{aligned} \tag{2.22}$$

To find the matching condition for this mode, the ratio of (2.22) is taken and the interface conditions (2.20) are applied, with some rearranging:

$$\frac{k_{1x}}{\epsilon_1} + \frac{k_{2x}}{\epsilon_2} = 0 \tag{2.23}$$

Finally, enforcing conservation of momentum in this two-dimensional system with $k_x^2 + k_z^2 = k_0^2 = (\omega^2 / c^2)\epsilon_{medium}$, we arrive at the dispersion relations:

$$k_z = k_0 \sqrt{\frac{\epsilon_1 \epsilon_2}{\epsilon_1 + \epsilon_2}} \tag{2.24}$$

$$k_{nx} = k_0 \sqrt{\frac{\epsilon_n^2}{\epsilon_1 + \epsilon_2}} \tag{2.25}$$

where k_{nx} is the propagation into the *n*th space in the *x* direction.

Now if one of the permittivities is metallic ($\mathrm{Re}\{\epsilon\} < 0$), say ϵ_1, then the only way this mode has a real k_z (and therefore propagates), is for $|\epsilon_1| > \epsilon_2$. The consequence is that k_{1x} and k_{2x} must both be imaginary. Therefore, components of this mode into those spaces must be evanescent and the mode itself will be a TM mode tightly confined to the plane of interface. The possibility of this mode is the key inspiration for the architectures described in this work.

The MOS Capacitor

The heart of modern electronics lies in the Metal Oxide Semiconductor transistor. Somewhat surprisingly, before one can explore the accumulation surface plasmon a basic understanding of MOS architecture is required. Recall that the controllable nature of a MOS transistor is in the creation of a conductive channel in what is otherwise an insulator. The conceptual basics of its operation are as follow: a metal gate, an insulating oxide and a doped silicon substrate are sandwiched on top of a ground plane as shown in Figure 2.3. For illustrative purposes, assume an n-type doped semiconductor and gold electrodes. A positive potential applied to the gate moves the free charges that define a metal, generating a net surface charge at the *metal-oxide* boundary. Doping in the silicon introduces free negative carriers; at equilibrium, these carriers are diffuse enough that conduction is limited, but when the bias is applied the dopant carriers are drawn to the *silicon-oxide* boundary forming the surface charge Φ_S. This potential varies with extent into the silicon and forms a conductive "metal-like" channel whose thickness is a function of many parameters such as dopant concentration and applied bias. Additionally, it should be recognized that, when the channel is active, this entire device can be viewed as a parallel plate capacitor whose capacitance is non-linear and will ultimately determine the time dynamics of the

switching operation. For our purposes a relationship between an applied bias and accumulation layer thickness is essential.

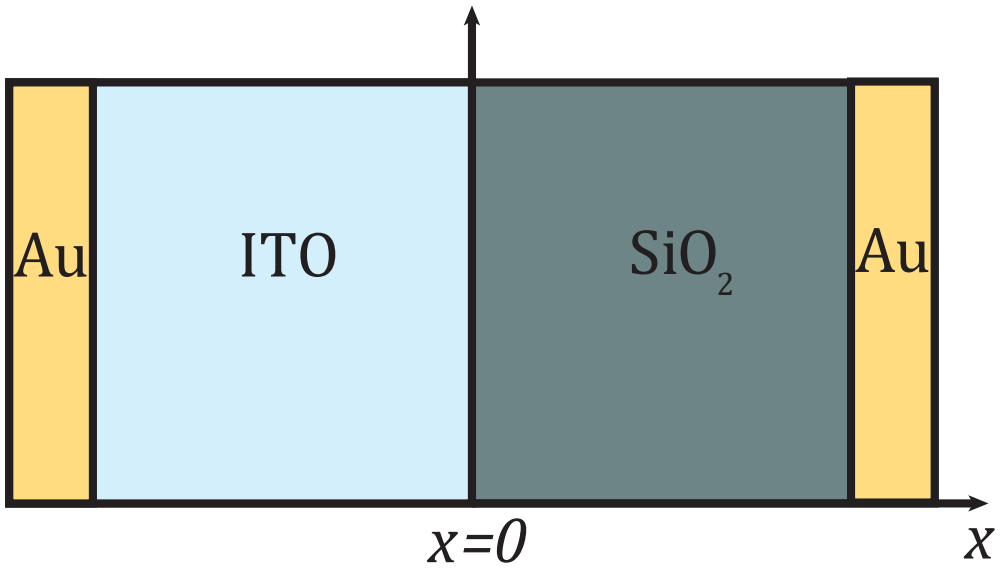

Figure 2.3: Notional Architecture of an ITO MOS Capacitor

Applying a positive voltage on the SiO_2 electrode of the structure causes electrons to accumulate at the ITO to SiO_2 interface. This charged accumulation layer has a spatial extent from $x = 0$ to $x = -x_{acc}$. Following analysis adapted from Colinge [10] the potential in the accumulation layer can be written as:

$$\Phi(x) = \Phi_T \ln\left[\sec^2\left(\frac{x_{acc} + x}{\sqrt{2}L_D}\right)\right] \tag{2.26}$$

Where L_D is the Debye length of the ITO and Φ_T is the thermal potential. Setting boundary conditions for the potential and expounding on the quantities, we can define the following:

$$\Phi_S = \Phi(0) \qquad \Phi_T = \frac{kT}{q}$$

$$\Phi(-x_{acc}) = 0 \quad L_D = \sqrt{\frac{\varepsilon_0 \varepsilon_{ITO} \Phi_T}{qN_d}}$$

Here, k is the Boltzmann constant, T is the ambient temperature in Kelvin, N_d represents the doping density of the ITO, q is the fundamental unit charge of an electron and ε_{ITO} is the static permittivity of the TCO.

Solving for the accumulation layer length from (2.26):

$$x_{acc} = \sqrt{2}L_D \arccos\left[\exp\left(-\Phi_S / \Phi_T\right)\right] \tag{2.27}$$

The electron density in the accumulation layer is given by [10]:

$$n(x) = N_d \exp\left(\frac{\Phi(x)}{\Phi_T}\right) \tag{2.28}$$

Substituting (2.26) into (2.28), we can establish an initial condition and a general formula for electron density :

$$\begin{aligned} n(x) &= N_d \sec^2\left(\frac{x_{acc} + x}{\sqrt{2}L_D}\right) \\ n(0) &= \frac{N_d}{\cos^2\left(\frac{x_{acc}}{\sqrt{2}L_D}\right)} = N_d \exp\left(\frac{2\Phi_S}{\Phi_T}\right) \end{aligned} \tag{2.29}$$

The total charge density dQ_A can then be found by integrating across the spatial extent of the accumulation layer electron density, which is composed of any electrons due to doping N_d, minus $n(x)$ from (2.29).

$$\begin{aligned} dQ_A &= \int_{-x_{acc}}^{0} qN_d - qn(x)dx \\ dQ_A &= qN_d\left[x_{acc} - \sqrt{2}L_d \tan\left(\frac{x_{acc}}{\sqrt{2}L_d}\right)\right] \end{aligned} \tag{2.30}$$

Replacing x_{acc} with the relation from (2.27), we can get the area differential charge as a function of only the surface potential:

$$dQ_A = qN_d\sqrt{2}L_D\left[\arccos\left(\exp\left(-\frac{\Phi_S}{\Phi_T}\right)\right)-\exp\left(\frac{\Phi_S}{\Phi_T}\right)\sqrt{1-\exp\left(-\frac{2\Phi_S}{\Phi_T}\right)}\right] \tag{2.31}$$

Since we are applying a bias voltage to the SiO_2 electrode, we know that the electric field in the SiO_2 region must satisfy the line integral of the potential difference between the electrode and the ITO/SiO_2 interface, where d is the length of the SiO_2 layer:

$$\left|\mathbf{E}_{SiO_2}\right| d = V_{Bias} - \Phi_S \tag{2.32}$$

At steady state, the charges in the SiO_2 will balance the charge associated with the accumulation layer; thus, the electric field in the SiO_2 will be:

$$\mathbf{E} = -\hat{\mathbf{x}}\frac{dQ_A}{\varepsilon_0\varepsilon_{SiO_2}} \tag{2.33}$$

Finally, substituting (2.33) and (2.31) into (2.32) and assuming that the surface potential is a weak function of the bias voltage ($V_{Bias} >> \Phi_S$), we can establish a relation between applied voltage and surface potential at the interface:

$$V_{Bias} = \Phi_S + \frac{qN_d\sqrt{2}L_D d}{\varepsilon_0\varepsilon_{SiO_2}}\left[\arccos\left(\exp\left(-\frac{\Phi_S}{\Phi_T}\right)\right)-\exp\left(\frac{\Phi_S}{\Phi_T}\right)\sqrt{1-\exp\left(-\frac{2\Phi_S}{\Phi_T}\right)}\right] \tag{2.34}$$

The above relation cannot be algebraically inverted to solve for Φ_S. Thus, when doing an analysis of this architecture, a numerical curve must be calculated.

Electro-Optical Modulators

As a rule, isolated sinusoids carry no information. Thus, for communication to occur it is often the case that baseband signals are mixed with a higher frequency carrier forming a complex envelope. RF signals can be easily mixed through a either a non-linear element or a switch and while the mixing of an RF signal onto an optical carrier entails a salient change in

phenomenological domain we can similarly partition the set of modulators that accomplish this mixing into two classes: electro-optic effect modulators and electroabsorptive modulators.

Electro-optic effect modulators rely on a medium whose optical propagation characteristic vary with an applied electric field. Namely, anisotropic non-centrosymmetric linear materials like $LiNbO_3$ experience a refractive index change with an applied field through the linear Pockels effect. *All* materials exhibit the quadratic Kerr effect, but require much higher field strengths [6] [11]. These effects are mentioned for completeness, but for the purposes of this work only electroabsorption will be explored.

Electroabsorption is a conceptually simple process: through some control signal, the loss of some medium can be varied. Thus, a light wave that propagates through this medium will have its intensity envelope modulated with the control signal. In the context of the MOS capacitor, injecting free carriers into the conduction channel formed at the interface, is an effective means of changing the optical loss of the channel. In the context of the parametrically "pumped" nanoparticles, radiation into the background medium is a net loss on the guided mode and, as shown in a later chapter, can be controlled. Although the pumping field itself is too high frequency to be electronic, the *presence* of this pump field could be electronically switched, leading to another potential architecture for electroabsorptive modulation.

Many proposed electroabsorptive modulator (EAM) architectures base their operation on complicated quantum scale effects [3] and have had limited application success. The architectures proposed in this work similarly approach the size and power goals of these more traditional EAM schemes without the conceptual complexity. We posit that due to the overall reduction in dimensions of a plasmonics based modulator (we will show that the MOS architecture dimensions, for example, are on the order of several wavelengths) the insertion loss

will be significantly smaller than current EOM devices. Although not as small as quantum dots and other quantum well devices [3], the tradeoff for complexity in the following proposed architectures may make the schemes more amenable to the eventual goal of a photonic integrated circuit.

Aside from temporal dynamics which will limit bandwidth, electro-optic modulators have two important parameters which we will quantify to motivate the importance of small physical dimensions: the insertion loss and the extinction ratio. Extinction ratio is defined in (2.35), where I_m is the intensity for some maximal modulation bias ("on" voltage) and I_0 is the intensity with no modulation applied ("off" voltage). Extinction ratio is an expression of *how modulated* our intensity envelope can be, with a higher number leading to *deeper* modulation and improved bit error rate in a communication system. In other words, the wider the gap in absorption coefficient values between the "on" state and the "off" state, the better the modulation performance. Generally speaking, decreasing a device's length requires a larger applied electric field to maintain the same modulation contrast and extinction ratio.

$$ER = \frac{\left|I_m - I_0\right|}{I_m} \qquad I_0 \le I_m \tag{2.35}$$

Insertion loss is another figure of merit defined in (2.36), it is the ratio of intensity "lost" compared to the input intensity. This loss will also be a function of length. It should be obvious that due to propagation loss, the longer a device is, the higher the insertion loss. Thus, a trade-space is produced between insertion loss and extinction ratio. Choosing a length to increase one will decrease the other.

$$IL = 1 - \frac{I_m}{I_{in}} \qquad I_0 \le I_m \tag{2.36}$$

Thus, if we manage to reduce the length of a device to decrease losses and improve packaging, a commensurate increase in modulation *depth* is required to maintain a designed for extinction ratio [12]. Due to the high mobility of carriers in doped ITO [12] and relatively large voltages that can be applied to ITO, the MOS architecture presented is also tunable for modulation quality by either increased doping or increased bias. This tunability further strengthens the argument for an ITO-MOS based modulator.

Chapter 3. The Accumulation Surface Plasmon

Transparent Conductive Oxides

To be able to exploit the MOS capacitor structure as an SPP waveguide, appropriate materials must be chosen that not only satisfy the dispersion relations but do so at some optical frequency relevant to an engineer. For the near-infrared region (NIR) around 1550 nm, various materials have been studied [13] as viable for plasmonic devices. Notably, gold and silver are used due to their low loss.

However, pure metals have fixed carrier concentrations and offer little flexibility in manufacturing. This means that finding a companion insulator can be challenging. TCOs, on the otherhand, can be manufactured to have a range of concentrations through doping and can be highly tunable through electric bias [14]. Furthermore, as will be shown, when coupled with a MOS architecture, TCOs open the possibility of actively switching between a dielectric regime and a plasmonic regime as a means of electro-absorptive modulation. At the same time, TCOs offer significantly lower optical loss in the NIR as shown in Figure 3.1**:** Imaginary parts of dielectric function of a) gold and b) various TCO films deposited using pulsed laser deposition.

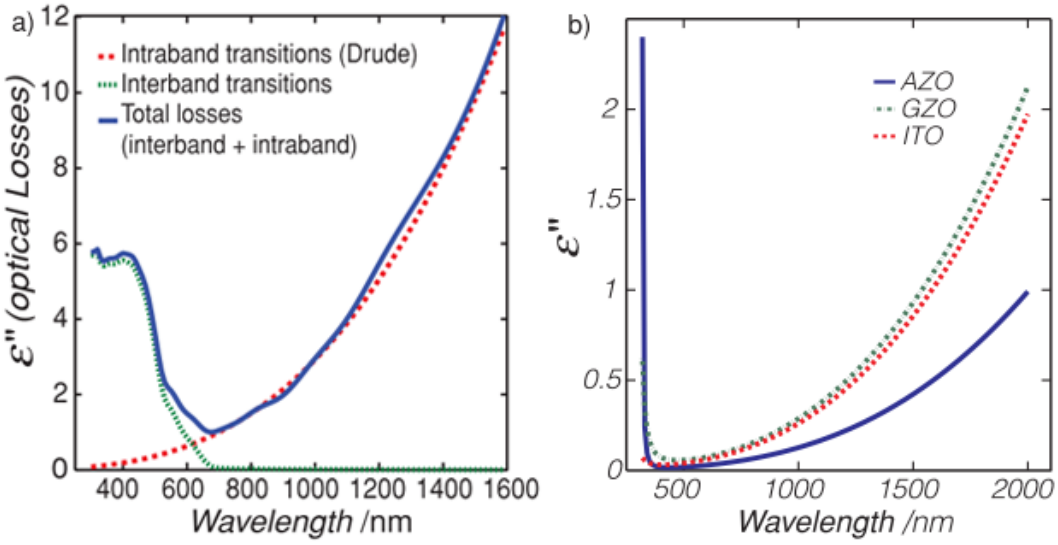

Figure 3.1: Imaginary parts of dielectric function of a) gold and b) various TCO films deposited using pulsed laser deposition. [13]

The Thin Film SPP

From equation (2.25) one can see that the rate of wave vector decay is controlled by the magnitude of the permittivities in the half spaces; that is the confinement of the mode is defined only by the materials. But, what if one were to try and "squeeze" the mode?

It has been shown [15] that by sandwiching the metal as a thin film between two dielectric spaces, one can control the confinement of an anti-symmetric plasmonic mode. As shown in Figure 3.2 c), the wave vector on the interface grows dramatically as the film thickness is diminishes for the antisymmetric mode. This implies that it is possible to squeeze a mode into a sub-wavelength waveguide, paving the way to electro-optical devices on the order of the wavelength [16].

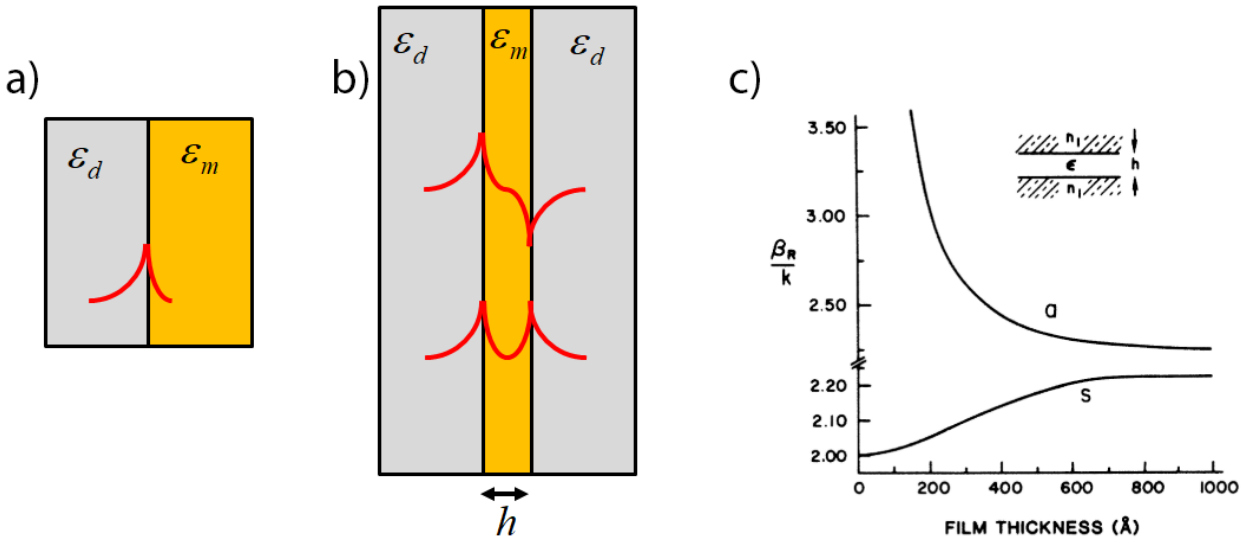

Figure 3.2: a) SPP model, b) Thin Film SPP Model, c) Dispersion relation for antisymmetric (a) and symmetric (s) modes of a thin-film SPP [15]

The consequence of this adds additional restrictions to the use of noble metals in plasmonic devices. Traditionally manufacturing thin films of gold will invariably introduce grain boundaries and interband transition states for these boundaries, potentially spoiling any desired plasmonic modes.

Virtual Thin Films and the ASP

The thin film geometry has been used as an approximation for previous analyses of ITO based MOS photonic devices [14], [17]. That is, charge density in the accumulation layer is assumed to have a uniform distribution and an effective permittivity. This "virtual thin film" accumulation layer is between 0 and x_{acc} in Figure 3.3. However, as will be shown, this approximation blurs some of the underlying physics.

By eschewing this assumption and adopting a perturbative approximation of the charge density, the spatial variation of permittivity in the accumulation layer as a function of voltage can

be rigorously derived. Since surface plasmons occur at boundaries between negative and positive permittivity, it is reasonable to assume that if such a transition can be established in an accumulation layer, then a plasmonic mode will exist. This mode, when present in the graded permittivity profile, is a novel phenomenon known as the Accumulation-layer Surface Plasmon (ASP) [18]. The analysis as follows is from [19] published in Optics Letters.

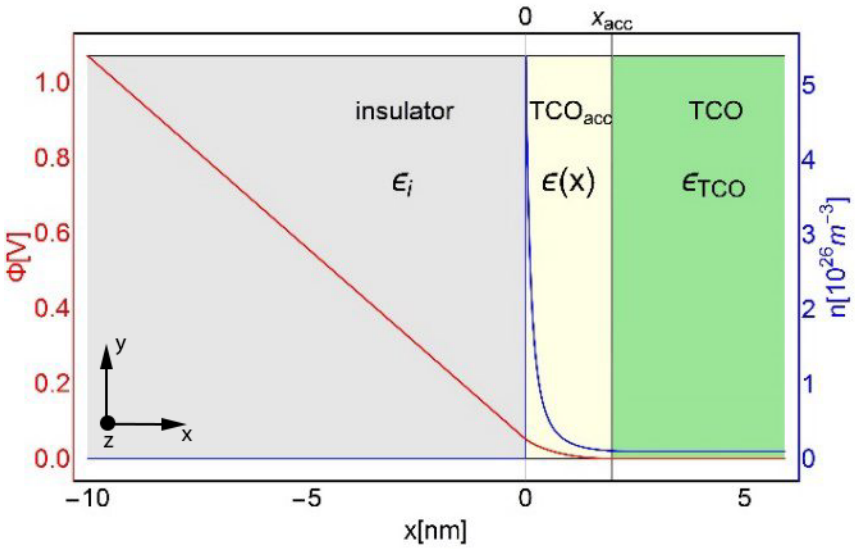

Figure 3.3: Electrostatic potential and charge density as a function of position in a Silicon-dioxide/ITO MOS structure. The ITO doping concentration is $N_d = 10^{25}$ m^{-3} and the applied bias is 1 V.

Analysis and Simulated Results

Using Eq. (2.27), Eq. (2.29) and the analysis steps that resulted in Eq. (2.19), we can arrive at a time harmonic Drude model of the permittivity function in the system denoted in Figure 3.3:

$$\varepsilon(x) = \begin{cases} \varepsilon_{TCO} + \delta_\chi \tan^2[(x - x_{acc}) / \left(\sqrt{2} L_D\right)] & 0 < x < x_{acc} \\ \varepsilon_{TCO} = \varepsilon_s + \delta_\chi & x > x_{acc} \end{cases} \tag{3.1}$$

Where $\delta_\chi = -\omega_p^2 / [\omega(\omega + i\gamma)]$, ε_s is the static TCO permittivity, and the plasma frequency of the unbiased ITO is $\omega_p = [N_d q^2 / (\varepsilon_0 m^*)]^{1/2}$, m* is the effective mass of an electron.

Using Eq. (3.1), and the parameters used by Naik et al [13], it can be shown that for different doping concentrations between 10^{26} m^{-3} and 10^{27} m^{-3} there are three distinct permittivity profiles that can be sustained. It should be noted that higher concentrations required higher bias voltages to maintain the ratio Φ_S / Φ_T around unity. The profiles can be categorized as the following cases:

1. Below a certain doping concentration, the real part of the permittivity is dielectric, with a positive, near-constant permittivity. Denoted by dashed blue in Figure 3.4.

2. If the doping concentration is high enough, the permittivity profile is negative everywhere and the ITO is metallic overall. Denoted by dash-dotted green in Figure 3.4.

3. With an intermediate concentration the permittivity profile starts out negative inside the accumulation layer then has a zero crossing into a positive permittivity across the accumulation layer and beyond. This not only promises the thin film like response desired, but also allows the exploration of Epsilon-Near-Zero (ENZ) regimes [20], [21] Denoted by the solid red curve in Figure 3.4.

It should be clear that case 1 will not exhibit interesting behavior since the entire device would just be an insulator with no plasmonic properties. Thus, only cases 2 and 3 will be considered for analysis.

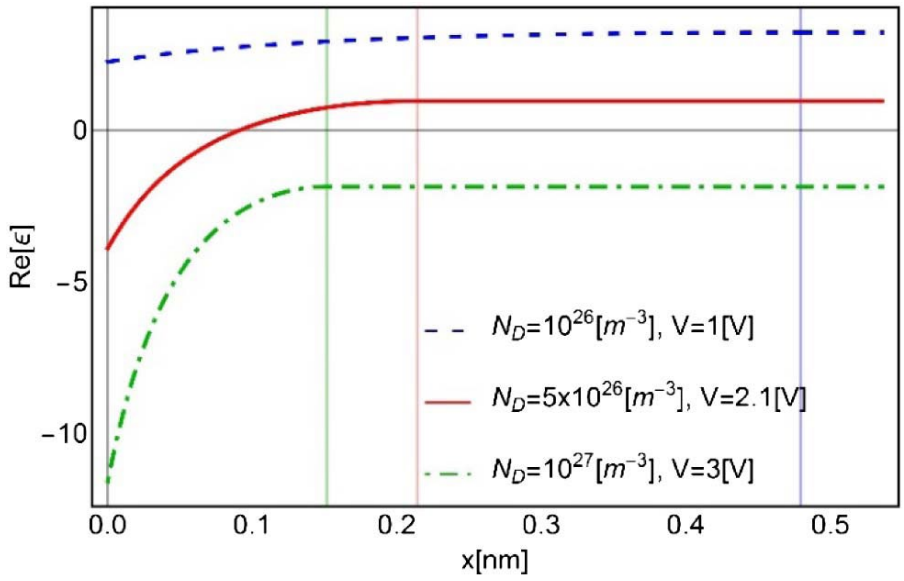

Figure 3.4: Permittivity profile in the accumulation layer in an ITO film with three different doping concentrations.

A surface plasmon propagating on an interface can be expressed purely as a function of the magnetic field component parallel to the interface. Thus, with reference to Figure 3.3, we only need to consider the TM wave propagating in the z direction along the y unit vector $\hat{\mathbf{y}}$:

$$\mathbf{H}(x,z) = \begin{cases} \hat{\mathbf{y}} H_0 e^{\alpha_i x} e^{i\beta z} & x < 0 \\ \hat{\mathbf{y}} H_y(x) e^{i\beta z} & x > 0 \end{cases} \tag{3.2}$$

Here H_0 is the complex amplitude of the magnetic field at the insulator-TCO interface, β is the phase constant and $\alpha_i = (\beta^2 - k_0^2 \varepsilon_i)^{1/2}$ is the attenuation constant for the wave in the insulator.

For case 3, the following equations and boundary conditions at *x=0* hold; note that the prime and double-prime notation denote the first and second differential of a function with respect to its argument.

$$H_y''(x) - [\frac{\varepsilon'(x)}{\varepsilon(x)}]H_y'(x) + [k_0^2\varepsilon(x) - \beta^2]H_y(x) = 0$$
$$H_y(0) = H_0 \tag{3.3}$$
$$H_y'(0) = H_0 \frac{\alpha_i \varepsilon(0)}{\varepsilon_i}$$

In case 3, the permittivity approaches ε_{TCO} as x approaches x_{acc}; thus $H_y(x)$ will approach $\exp(-\alpha_{TCO}x)$ as x approaches x_{acc}, where $\alpha_{TCO} = (\beta^2 - k_0^2\varepsilon_{\mathrm{TCO}})^{1/2}$. This leads to a third boundary condition, this time at the $x=x_{acc}$ boundary:

$$H_y'(x_{acc}) = \frac{-H_y(x_{acc})\alpha_{TCO}\varepsilon(x_{acc})}{\varepsilon_{TCO}} \tag{3.4}$$

Rather than finding solutions to the differential equation in (3.3), it is preferable to enforce the boundary conditions in (3.3) along with (3.4) since it restricts the solution space to the range $0<x<x_{acc}$.

In case 2 the permittivity is negative throughout the entire TCO layer, the differential equation in (3.3) has no inflection points and thus is fully integrable. This lends to function to solution by numerical techniques such as Runga-Kutta [22] or shooting method [23] Runga-Kutta would be applied to an IVP consisting of (3.3), shooting would allow us to find β satisfying Eq. (3.4). However, numerical solutions require a priori choices of various experimental parameters and can create a loss of generality, thus any treatment would be amiss without an attempt at an analytical solution.

In general, the differential equation in (3.3) cannot be integrated, but a perturbative method could be employed. Since the accumulation layer thickness, x_{acc}, is much shorter than our wavelength, the spatial variations of the magnetic field over the accumulation layer are expected to be dictated by the fast spatial variation of the permittivity profile $\varepsilon(x)$ rather than by wave

dynamics represented by the first order term of Eq. (3.3). This allows us to neglect such a term and obtain the following approximate equation for the magnetic field within the accumulation layer:

$$H_y''(x) - [\frac{\varepsilon'(x)}{\varepsilon(x)}]H_y'(x) = 0 \tag{3.5}$$

Integrating (3.5) two successive times:

$$\begin{gathered} H_y'(x) = A_1\varepsilon(x) \\ \downarrow \text{ integrate} \\ H_y(x) = A_2 + A_1\int_0^x \varepsilon(s)ds \end{gathered} \tag{3.6}$$

Then, applying the boundary conditions from (3.3) and solving for A_1 and A_2,:

$$\begin{aligned} &H_y(0) = H_0 \\ &H_y'(0) = \frac{\varepsilon(0)}{\varepsilon_i}\sqrt{\beta^2 - k_0^2\varepsilon_i}H_y(0) \\ &\rightarrow H_y(x) = H_0 + \frac{\sqrt{\beta^2 - k_0^2\varepsilon_i}}{\varepsilon_i}H_0\int_0^x \varepsilon(s)ds \end{aligned}$$

Then, inserting permittivity function (3.1) and integrating we get the closed form solution for the field:

$$H_y(x) = H_0\left(\frac{\varepsilon_i + (\varepsilon_{TCO} + \delta_\chi)\sqrt{\beta^2 - k_0^2\varepsilon_i}\,x + \sqrt{\beta^2 - k_0^2\varepsilon_i}\sqrt{2}L_d\delta_\chi\left[\tan\left(\frac{x_{acc}}{\sqrt{2}L_d}\right) + \tan\left(\frac{x - x_{acc}}{\sqrt{2}L_d}\right)\right]}{\varepsilon_i}\right) \tag{3.7}$$

This solution holds in the accumulation layer width $0<x< x_{acc}$. Outside of the accumulation region the permittivity is ε_{TCO} and the field is of the form:

$$H_y(x) = H_y(x_{acc})\exp\left(-\alpha_{TCO}(x - x_{acc})\right) \tag{3.8}$$

Then, applying the boundary condition in (3.4) we get:

$$H_0 \frac{\varepsilon_{TCO}\sqrt{\beta^2 - k_0^2 \varepsilon_i}}{\varepsilon_i} = -H_y(x_{acc})\sqrt{\beta^2 - k_0^2 \varepsilon_{TCO}} \tag{3.9}$$

Finally, we can solve (3.9) through a perturbation on the parameter x_{acc}/λ up to the first order that is, as we show later, accurate at wavelengths outside of resonance (i.e. $\varepsilon_{TCO}+\varepsilon_i=0$):

$$\beta = \beta_0 + \frac{\beta_0^3 \left(x_{acc}\varepsilon_s + \sqrt{2}L_d \delta_\chi \tan\left(\frac{x_{acc}}{\sqrt{2}L_d} \right) \right)}{k_0 \sqrt{(\varepsilon_{TCO}^2 - \varepsilon_i^2)(\varepsilon_i - \varepsilon_{TCO})}} \tag{3.10}$$

This acts as our perturbed dispersion relation across the accumulation layer, with $\beta_0 = k_0\sqrt{(\varepsilon_i \varepsilon_{\mathrm{TCO}})/(\varepsilon_i + \varepsilon_{\mathrm{TCO}})}$ being the dispersion relation at the interface between the insulator and TCO, $x=0$.

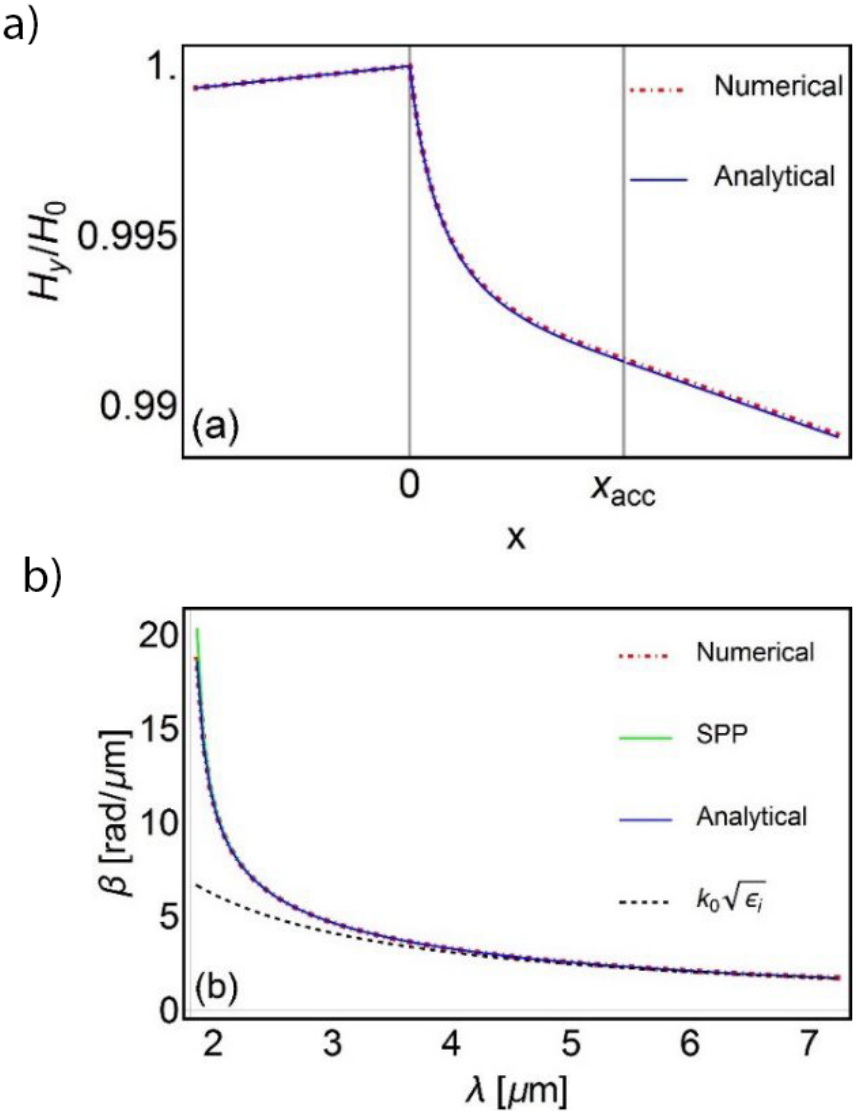

Figure 3.5: (a) Magnetic Field Profile and (b) β of an ASP in a SiO2–ITO MOS structure with doping concentration $N_d=10^{27}[m^{-3}]$ and surface potential $\Phi_S = 3\Phi_T$

As we can see from Figure 3.5, there is excellent agreement between the numerical shooting method solution and the analytically derived eigenmodes, which we believe can support ASP. Interestingly enough, the dispersion relation for our ASP and that of a surface plasmon polariton (SPP) which would exist in an unbiased, static material, are nearly identical. However,

this phenomenon breaks down as we approach resonance since the strong localization of fields causes the carrier density to have a much greater effect on ASP dispersion.

The solid curves in Figure 3.6 show the normalized propagation constant and the normalized propagation length of an ASP near resonance as a function of the surface potential obtained by solving the exact Eq. (3.9). By comparison the long-dashed curves show that, as expected, the perturbative approximation in Eq. (3.10) is no longer accurate near resonance. The dotted curves in Figure 3.6 correspond to the propagation of an SPP in the absence of the accumulation layer. The large excursion in the ASP propagation constant as a function of the applied electric bias makes these surface-wave modes interesting candidates for the realization of ultra-compact phase modulators.

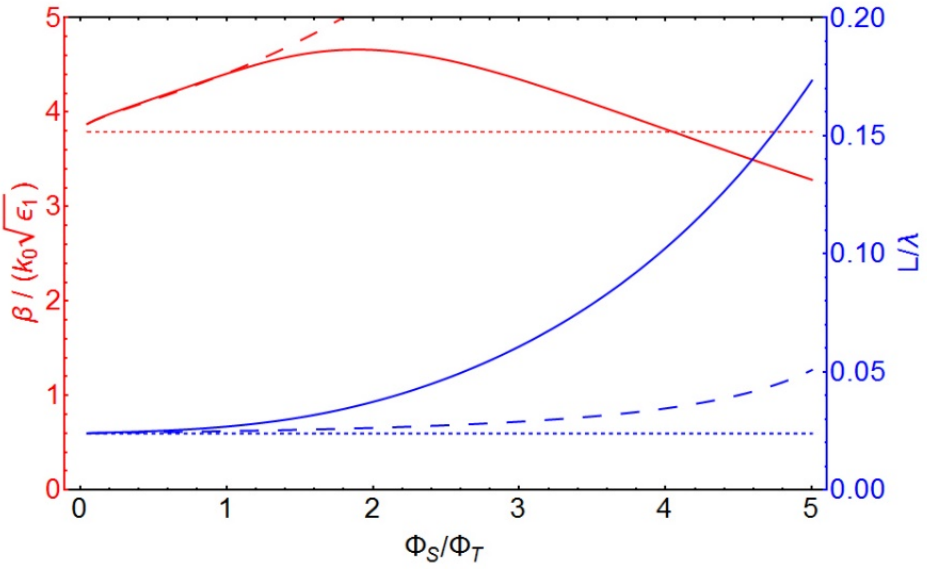

Figure 3.6: Normalized Propagation Constant and propagation length of the ASP in a SiO2–ITO MOS structure

Care must be taken when analyzing the properties of the case 3 system, in which the real part of the permittivity is negative within a portion of the accumulation layer and smoothly transitions

to a constant, positive value ε_{TCO} beyond the accumulation layer ($x > x_{acc}$). This is a unique situation, as within the same medium three distinct electromagnetic responses coexist: plasmonic near the interface with the insulator, dielectric within the TCO bulk, and ENZ in between [20]. In this case, using an averaging technique and assuming a uniform charge density to find the permittivity (which is the standard in MOS capacitor analysis), will lead to erroneous conclusions. A uniform plasmonic region of thickness x_{acc} and negative permittivity ε_p sandwiched between two distinct dielectrics with positive permittivities ε_i and ε_{TCO}, such that $|\varepsilon_p| > \max(\varepsilon_i, \varepsilon_{TCO})$ will support at least one mode [15], with the remarkable property of displaying more confinement (i.e., higher β) as the film thickness is reduced (until the resonance condition is met). As shown in the following, due to the existence of an ENZ region, an ASP mode is not supported by the accumulation layer.

The numerical methods (Runga-Kutta and shooting method) applied to Eq. (3.3) do not show any surface-bound eigenmodes. Thus, some other mechanism must be suppressing an ASP mode. But, by making the assumption that the permittivity in the accumulation layer is purely real and the permittivity profile is linearized around the point x_0 where $\varepsilon(x_0)=0$, we know that Eq. (3.3) has a singular point at x_0. A solution can thus be obtained using a Frobenius series [24]:

$$H_y(x) = (x - x_0)^{\gamma} \sum_{n=1}^{\infty} A_n (x - x_0)^n \tag{3.11}$$

The parameter γ in this equation is one of the two roots of the indicial polynomial P(γ) associated with the Frobenius series solution of Eq. (3.3). To fulfill the boundary conditions (3.3) and (3.4) a second linearly independent solution associated with the second root of the indicial polynomial must be obtained. Under the present assumptions P(γ) has two identical roots, so it can be shown that the second solution has a logarithmic singularity at x_0. Because of its singular nature such a

second solution must be discarded as unphysical, and therefore no guided eigenmodes exist in this case.

In conclusion, a rigorous analytical study of the eigenmodes supported by a charge accumulation layer was presented. The new class of surface plasmons termed ASP was introduced. Near resonance ASPs display high tunable within the regime, allowing for calibration of the effective index through bias application. Additionally, the phenomenon of ENZ in the accumulation layer could play a supressory role on ASP production, and it was considered. The present analytical results could provide important guidelines for the design of ITO-based optoelectronics devices.

Chapter 4. Parametric Plasmonic Resonance

Parametric Resonance

The harmonic oscillator is arguably the most fundamental building block for understanding the mechanics of photonic systems. However, as is evinced by our analysis of the Drude theory in Chapter 2, we typically only consider two types of oscillations: natural oscillations and driven oscillations. This is unsurprising, since the solution of any driven, damped, time invariant system is composed of two terms: transients, whose oscillatory period depend on the natural period (albeit decaying); and the steady-state, which will be at the same angular frequency as the driving oscillation. When the external, driving frequency and the natural frequency are near each other *resonance* occurs and the amplitude of the response is maximized.

For some arbitrary second order driven differential equation:

$$m\frac{d^2x(t)}{dt^2} + k\frac{dx(t)}{dt} + cx(t) = F_0 e^{j\omega t} \tag{4.1}$$

Some particular solution will be of the form, $x(t) = \mathrm{Re}[Ae^{i\phi}e^{i\omega t}]$ and the amplitude:

$$A = \frac{F_0}{(c - m\omega^2)^2 + k^2\omega^2} \tag{4.2}$$

Which is clearly maximized when $\omega = \sqrt{c/m} = \omega_0$, which is the natural frequency [25].

However, an alternative way for growing the amplitude of the response exists: when the system is *not* time-invariant and some system *parameter* is also a periodic function of time. The most intuitive example of this is a child standing on a swing: after being given some initial push, a child can "pump" energy into his swing oscillation by squatting at the bottom of the swing and standing at the peaks. This temporally varies the inertia of the classical pendulum oscillator by

effectively modulating the length of the pendulum at a period of T/2 where T is the natural period of the swing and will amplify the total oscillation.

To further elucidate this phenomenon, consider the case of a prototypical RLC circuit, with a capacitance that is externally controllable and can be time-varying:

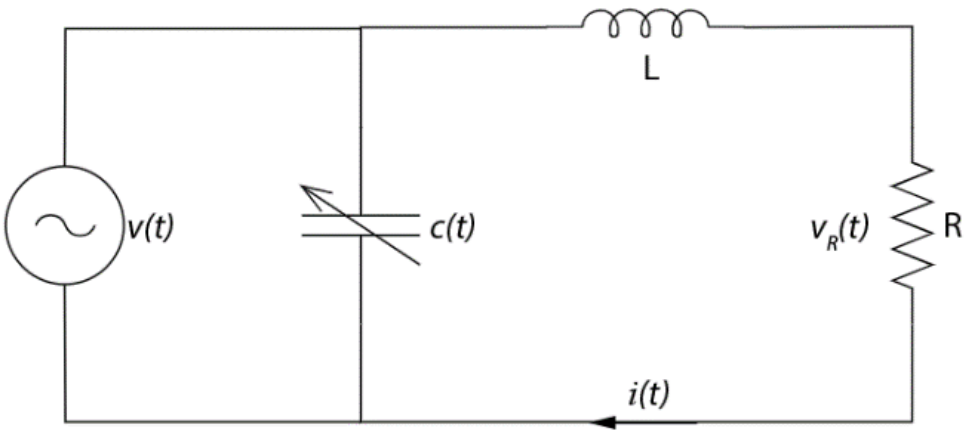

Figure 4.1: Time Varying RLC circuit

Suppose we wish to measure the amplitude of $v(t)$, the voltage across the load, by varying the non-linear capacitance $c(t) = C(1 + a_0 \cos(\omega_c t))$ with some function of frequency ω_c (this form is chosen for analysis). Beginning with the differential equations for the reactive components, ignoring the time varying nature of the capacitor and summing the voltages around the loop:

$$v(t) - L\frac{di(t)}{dt} - i(t)R = 0$$

$$v(t) + LC\frac{d}{dt}\left(\frac{dv(t)}{dt}\right) + C\left(\frac{dv(t)}{dt}\right)R = 0 \tag{4.3}$$

We arrive at a familiar undriven harmonic oscillator equation:

$$\frac{d^2}{dt^2}v(t)+\frac{R}{L}\frac{d}{dt}v(t)+\frac{1}{LC}v(t)=0 \tag{4.4}$$

Now, inserting the time varying capacitance and recognizing that $\omega_0 = 1/\sqrt{LC}$, we can arrive on a damped Mathieu equation [26]:

$$\frac{d^2}{dt^2}v(t)+\frac{R}{L}\frac{d}{dt}v(t)+\left(\omega_0^2[1+a_0\cos(\omega_c t)]\right)v(t)=0 \tag{4.5}$$

Essentially, the natural frequency of the system (normally ω_0) has been modulated. Assuming aligned phases between the parametric function and oscillation, the solution stability boundary includes $v(t)=\cos(1/2\, w_c t)$ and the amplitude will grow (overcome the damping) when $a_0 > 2RC/(\omega_0 L)$ [27]. Thus, some arbitrary mode in $v(t)$ can be excited by parametrically varying some other parameter of the system.

Multipolar Modes

Given this understanding of parametric resonance, we are now motivated to apply it to plasmonic architectures. In particular, we study the energy exchanges between a plasmonic nanoparticle and a time varying background medium [28]. Traditionally, only the lowest order dipolar modes are accessible for coupling with incident radiation. Although other modes theoretically exist, they require spatial variations much smaller than the wavelength. In addition, these modes are difficult to verify experimentally. By reciprocity, if we can't couple to them, then they are also weak "sub-radiant" emitters; ergo, the local field excitation never makes it into the far field for a detector to see. As will be analytically shown, these multipolar, high order modes *can* be accessed through parametric resonance in a phenomenon termed Plasmonic Parametric Resonance (PPR) [28], [29].

Efficient mechanisms for the delivery of energy to the nanoscale are important to achieve the strong local fields necessary to boost light-matter interactions, for enhanced nonlinear optics, for sensing and spectroscopic applications and for overall miniaturization of devices. As shown in the previous chapter, surface plasmons have been extensively exploited for such purpose. Localized surface plasmons (LSPs) are non-propagating coherent oscillations of free-carriers coupled to the electromagnetic field arising as a consequence of confinement effects in sub-wavelength nanoparticles. These modes can be excited through optical or electronic scattering and lead to strongly localized electric fields in proximity of the nanoparticle. An enhanced optical response is obtained when LSPs are excited at the resonant frequency of the electric dipole mode. While higher order eigenmodes exist, they are essentially decoupled from the incident field. The resonant conditions for low-order resonances are strongly dependent on the geometry of the plasmonic nanostructure. On the other hand higher order modes tend to occur around frequencies for which ε_1, the permittivity of the particle is nearly the opposite of ε_2, the permittivity of the surrounding medium. This should not be surprising, as it is analogous to the permittivity requirements for the ASP in Chapter 3. The spectral distribution of the modes of a plasmonic nano-sphere is illustrated in Figure 4.2 a).

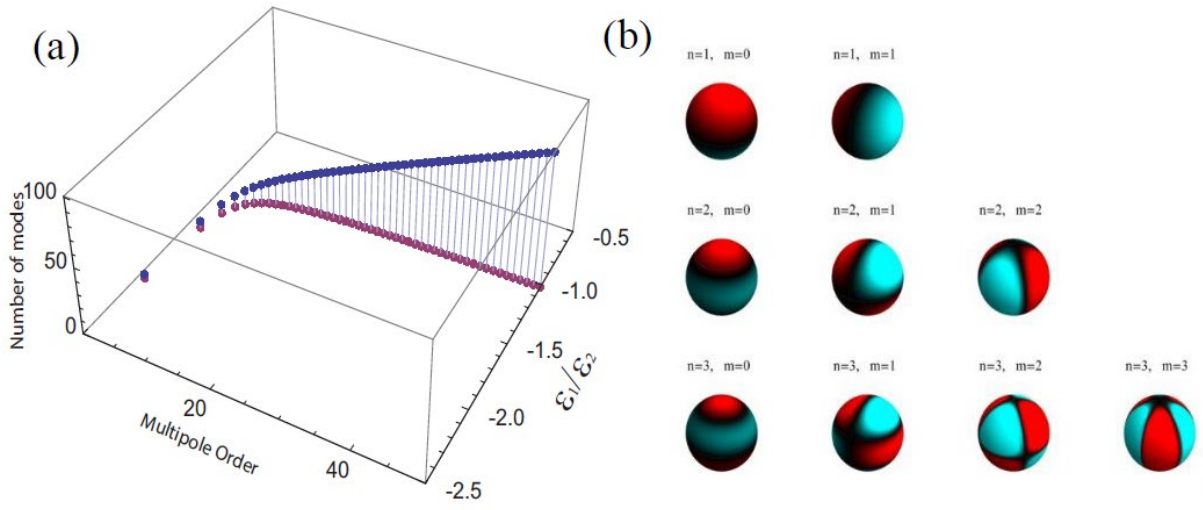

Figure 4.2: a) Spectral distributions of the resonant modes of a plasmonic nanosphere. b) Surface polarization charge density for the first few modes of a plasmonic nanosphere.

What makes the efficient optical excitation of high order modes in plasmonic nanostructures a difficult endeavor is the fact that it requires significant spectral and spatial overlap between the incident field and the mode to be excited. While the availability of broad-band light sources makes the spectral overlap requirement rather easy to fulfill, matching the spatial field distribution poses a far more complex challenge, as in principle it would require an illumination which is structured over subwavelength length-scales. This requirement is evidenced again in the case of a spherical particle by the complex distribution of the surface polarization charge of the resonant modes shown in Figure 4.2 b). The fact that far-field illumination by means of homogeneous plane wave spectra is ineffective in exciting high order scattering modes can be easily understood in the case of spherical scatterers – the case of general targets can be handled similarly using the T-matrix formalism [30] and yields a similar qualitative behavior. To this end let us consider the spherical multipole decomposition of a plane wave in spherical coordinates [31]:

$$e^{ikz} = e^{ikr\cos(\theta)} = \sum_{n=0}^{\infty} i^n (2n+1) j_n(kr) P_n(\cos(\theta)) \tag{4.6}$$

In equation (4.6) $k = 2\pi/\lambda$, λ is the wavelength in the background medium, $j_n(k,r)$ is a spherical Bessel function of the first kind of order *n,* and $P_n(\cos\theta)$ is a Legendre polynomial of degree *n*. Whereas multipoles of arbitrarily high order are present in the decomposition (4.6), their ability to effectively interact with a scatterer depends on their amplitude over the volume of the scatterer itself, as schematically illustrated in Figure 4.3.

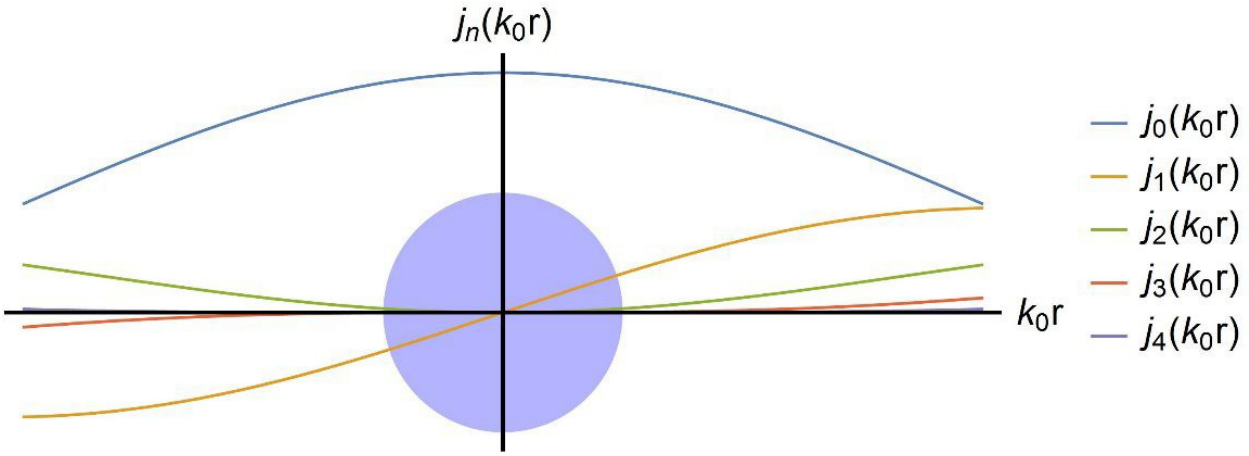

Figure 4.3: Interaction of various incident spherical harmonics with a subwavelength particle.

In particular for a multipole of order *m*, in the limit of $k\,r \to 0$ (i.e. $r \ll \lambda$), the corresponding spherical Bessel function [32] has the asymptotic form $j_n(kr) \sim (2kr)^n\, n!/(2n+1)!$. Therefore we can estimate that for a particle with maximum linear dimension $R \ll \lambda$, the contribution of the incident field towards the excitation of a mode of order *n* decreases with modal order as $(R/\lambda)^n$.

Figure 4.4 shows a cross sectional partitioning of the modal scattering from a nano-sphere as dictated by (4.6). Again, although all modes may be present, their individual contributions are difficult to dissect from the sum; i.e. the mode is difficult to sense or couple to.

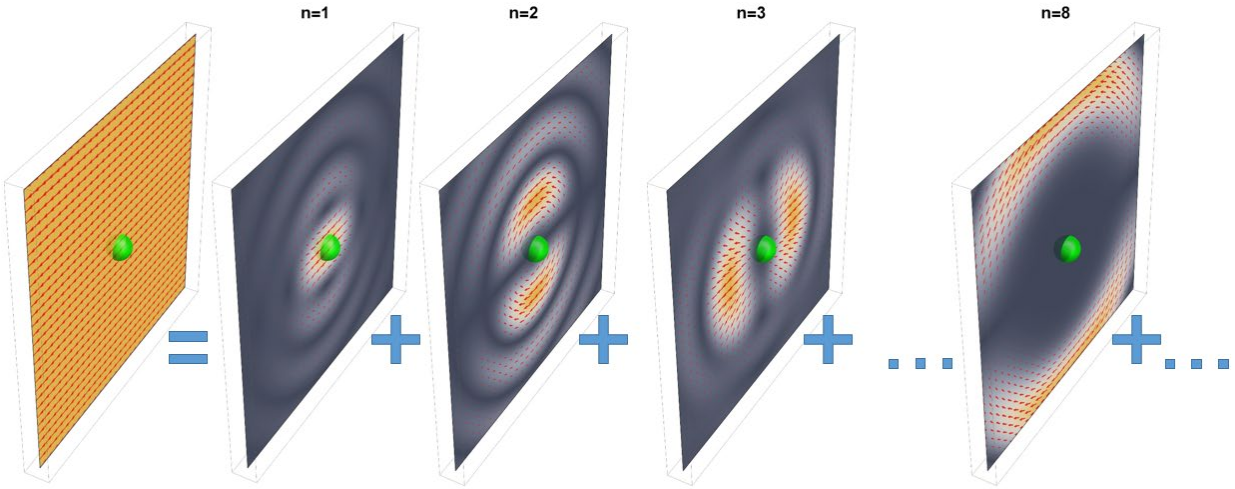

Figure 4.4: Scattering from a spherical particle partitioned by angular momentum order

Some of these difficulties could be overcome by exploiting the resonant dipolar scattering from a second particle positioned in the near-field of the particle in which the high order resonant mode is to be excited. The efficiency of such scheme may be estimated by means of the translation theorem for vector spherical harmonics [33]. While such approach can prove effective, nevertheless other issues arise because of the presence of the second particle to mediate the excitation of the high order resonant mode. In particular the spectral response of the original structure can be significantly modified due to coupling effects. Moreover, from a practical point of view the accurate positioning of the second particle may not be trivial in a variety of scenarios, like for instance colloidal systems.

Here we would like to describe a novel scheme for the excitation of high order localized surface plasmon [28] [29], which relies on a spatially uniform pump field in the presence of an

optical nonlinearity of the background medium in order to promote a process of resonant difference frequency generation that transfers energy to the desired plasmonic mode. In the next sections we present the analysis for a spherical particle.

Polarization Density in a Plasmonic Nanoparticle

In this section we derive the time-domain evolution equation for the polarization density in a plasmonic nanoparticle. From this point on a nanosphere of radius R is chosen to be the plasmonic particle for illustrative purposes. For a particle of deeply subwavelength dimensions the electric field spatial distribution can be obtained in the quasi-static approximation. In this regime the eigenmode of order n, m shows the following electric field spatial distribution:

$$\mathbf{E}_{nm}(\mathbf{r},t) = -E_n(t)\sqrt{\frac{2n+1}{4\pi}\frac{(n-m)!}{(n+m)!}}\nabla\left[Y_n^m(\theta,\phi)\begin{cases} \dfrac{r^n}{R^{n-1}} & r<R \\ \dfrac{R^{n+2}}{r^{n+1}} & r>R \end{cases}\right] \tag{4.7}$$

In equation (4.7) the function $Y_n^m(\theta,\phi)$ is the spherical harmonic function of integer degree n and integer order m as defined in [34]. The time-dependent parameter $E_n(t)$ is the time-varying amplitude of the mode to be determined. In the absence of an incident field the modal field (4.7) can satisfy the appropriate continuity boundary conditions for $r=R$ if and only if the following resonance condition is met:

$$\varepsilon_1 = -\frac{1+n}{n}\varepsilon_2 \tag{4.8}$$

Given the permittivity dispersion characteristics of the constituent media, equation (4.8) determines the resonant frequency of each resonant mode of the system. Here we assume a

constant permittivity ε_2 for the background medium and a Drude model for the nanosphere permittivity of the form:

$$\varepsilon_1(\omega) = \varepsilon_\infty - \frac{\omega_p^2}{\omega(\omega + i\gamma)} \tag{4.9}$$

In equation (4.9) ω_p is the plasma frequency of the plasmonic medium, γ is the collision frequency, and the non-dispersive component ε_∞ takes into account the presence of higher frequency spectral features. Under these assumptions the resonant frequency for a mode of order *n* is given by:

$$\omega_n = \sqrt{\frac{n\omega_p^2}{\varepsilon_2 + n\left(\varepsilon_2 + \varepsilon_\infty\right)} - \left(\frac{\gamma}{2}\right)^2} - i\left(\frac{\gamma}{2}\right) = \Omega_n + \mathrm{i}\Gamma_n \tag{4.10}$$

Considering the modal distribution (4.7) and the material dispersion (4.9) it is possible to write the dispersive portion of the polarization density within the volume of the nanosphere as:

$$\mathbf{P}_1(\mathbf{r},t) = P_n(t)\sqrt{\frac{2n+1}{4\pi}\frac{(n-m)!}{(n+m)!}}\nabla\left[\frac{r^n}{R^{n-1}}Y_n^m(\theta,\phi)\right] \tag{4.11}$$

It is straightforward to show that the time dependent amplitude $P_n(t)$ of the polarization density (4.11) obeys the following equation of motion for a damped harmonic oscillator:

$$\frac{d^2}{dt^2}P_n(t) + \gamma\frac{d}{dt}P_n(t) + \frac{n\omega_p^2}{\varepsilon_2 + n\left(\varepsilon_2 + \varepsilon_\infty\right)}P_n(t) = 0 \tag{4.12}$$

The solution of equation (4.12) is straightforward and related directly to the following interpretation of the total energy in the system as a superposition of potential energy of the polarization charges and kinetic energy of the polarization currents:

$$W_n(t) = \underbrace{\frac{nR^3}{2}\frac{1}{2\omega_p^2\varepsilon_0}\left(\frac{\partial P_n}{\partial t}\right)^2}_{Kinetic} + \underbrace{\frac{nR^3}{2}\frac{nP_n^2}{2\varepsilon_0\left(\varepsilon_2 + n\left(\varepsilon_2 + \varepsilon_\infty\right)\right)}}_{Potential} \tag{4.13}$$

Since the system behaves like a damped harmonic oscillator, the stored energy (4.13) decreases exponentially over time, while being periodically converted from potential to kinetic and back, depending on whether the polarization charge density or the polarization currents are maximum at for some given point in time. The temporal evolution of an octupolar mode ($n = 3$) is shown in Figure 4.5.

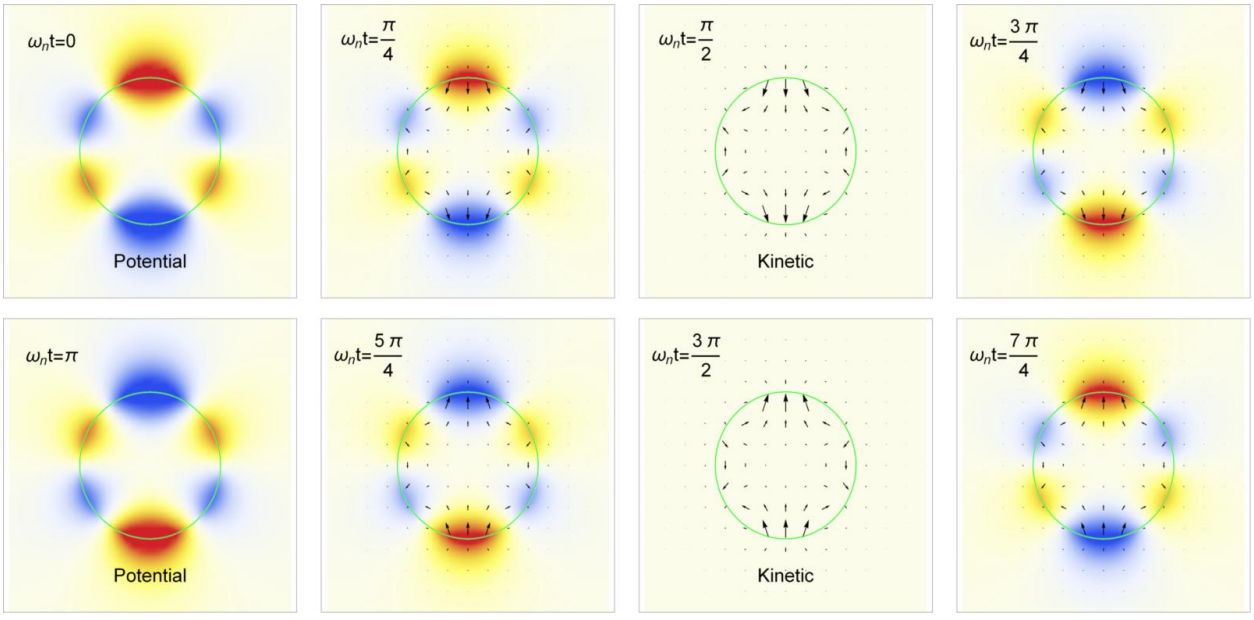

Figure 4.5: Temporal evolution of the potential and polarization currents of the octupolar mode of a plasmonic nanosphere

Tracing the evolution of a plasmonic eigenmode in the phase-space coordinate plane $\{P_n, \partial_t P_n\}$ leads to an inward spiral trajectory, due to absorption and radiation losses, as shown in Figure 4.6.

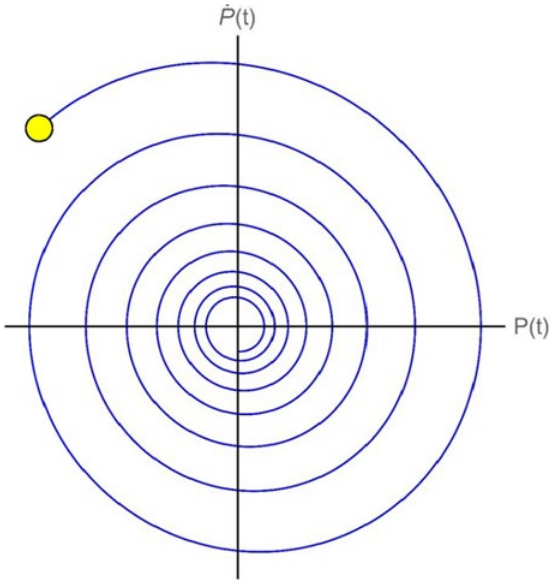

Figure 4.6: Phase-space trajectory of an attenuated eigenmode

A simple inspection of the energy expression (4.13) reveals an explicit dependence of the potential energy component on the permittivity ε_2 of the background medium. This feature is exploited in the next section to devise a pumping scheme able to transfer energy to any desired mode.

Background Permittivity Modulation

In this section we study the effects of a spatially uniform and temporally periodic modulation of the background permittivity ε_2. To simplify the analysis, we consider in particular the ideal case of a square wave modulation of the background material permittivity. The more realistic

sinusoidal modulation case leads to qualitatively similar results. If the temporal periodicity is judiciously chosen to lower ε_2 when the potential energy is maximum, while restoring it to its initial value when the potential energy is zero, power can be efficiently transferred to any resonant mode of the structure. The optimal repetition frequency for such a square wave is twice the resonant frequency of the relevant mode, consistent with the dynamics of a difference frequency generation process and with the conclusion of the discussion on page 33.

With the proposed scheme, radiative and dissipative losses of a mode can be compensated provided that a modulation depth threshold is reached or exceeded, in which case the amplitude of the modal oscillation would actually grow cyclically. In the case of our square-wave modulation scheme, the background medium's permittivity threshold would be approximately:

$$\frac{d\varepsilon_2}{\varepsilon_2} \sim \left(1+\frac{\varepsilon_\infty}{\varepsilon_2}\right)\frac{\pi}{Q_n} \tag{4.14}$$

In equation (4.14) Q_n is the quality factor for a plasmonic mode of order *n*. An example of the temporal evolution of the energy in the system when the threshold (4.14) is exceeded is shown in Figure 4.7 a). As a comparison, the consequences of not meeting the modulation threshold are shown in Figure 4.7 b), although the correct mode is coupled to by using the correct temporal dynamics in all three of the modulated traces, the only exponentially growing solution is one that is explicitly above the (4.14) threshold.

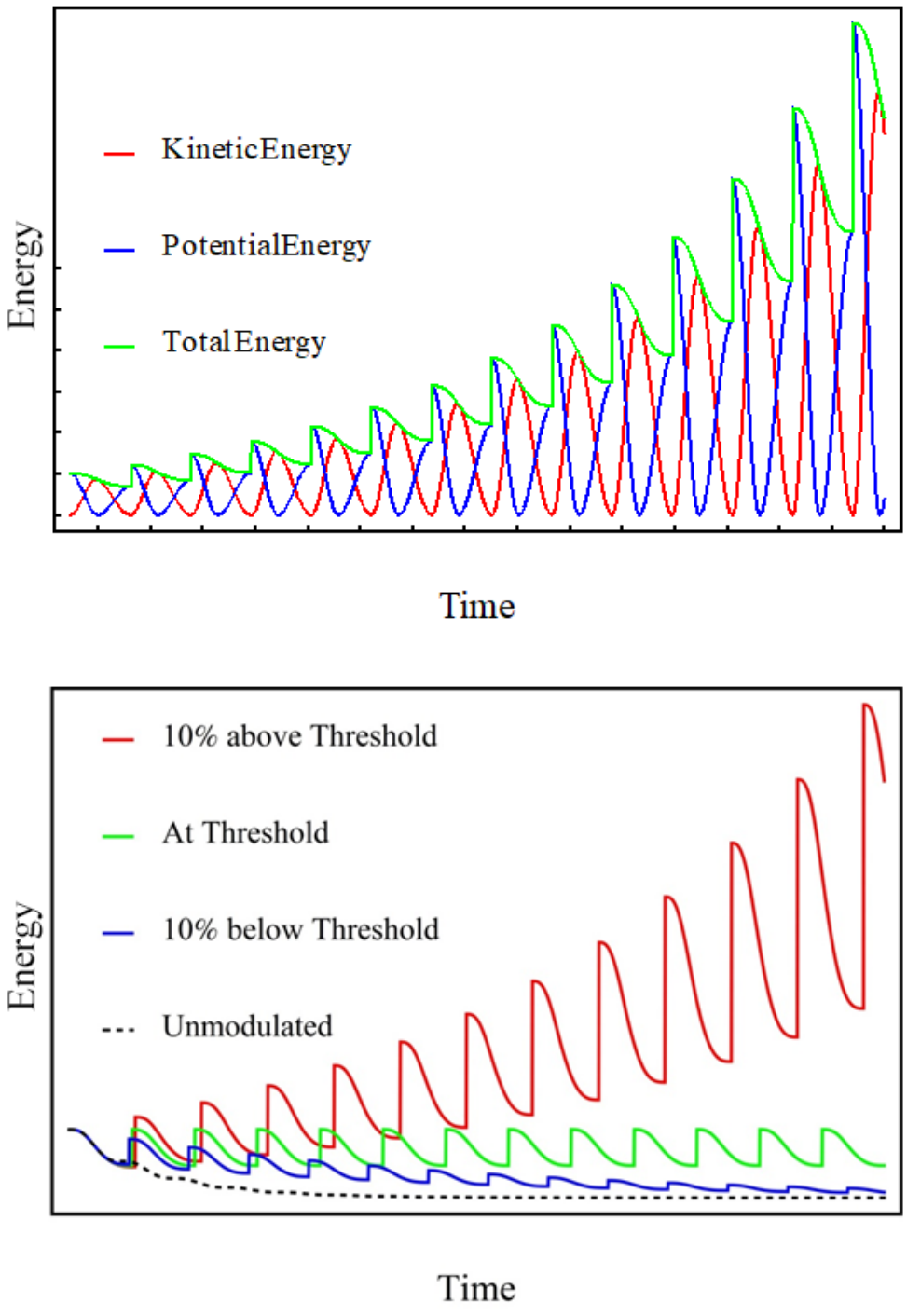

Figure 4.7: a) Temporal evolution of the stored energy in the octupolar mode of a plasmonic nanosphere when the background permittivity modulation depth has been exceeded and b) total energy dynamics as a function of modulation depth

The threshold condition (4.14) is obtained by following the scheme presented in Figure 4.8 through one full period of the plasmonic mode oscillation. The background permittivity ε_2 is modified so as to change the eigenfrequency from Ω_n to a smaller value Θ_n when the system is in a state of zero potential energy and maximum kinetic energy. The background permittivity ε_2 (and therefore the eigenfrequency of the mode) is restored to its original value when the system is in a state of maximum potential energy. This modulation step transfers energy to the plasmonic system and is exploited to counteract the modal attenuation. When allowed to proceed, this will lead to unstable amplitude growth of the desired plasmonic mode.

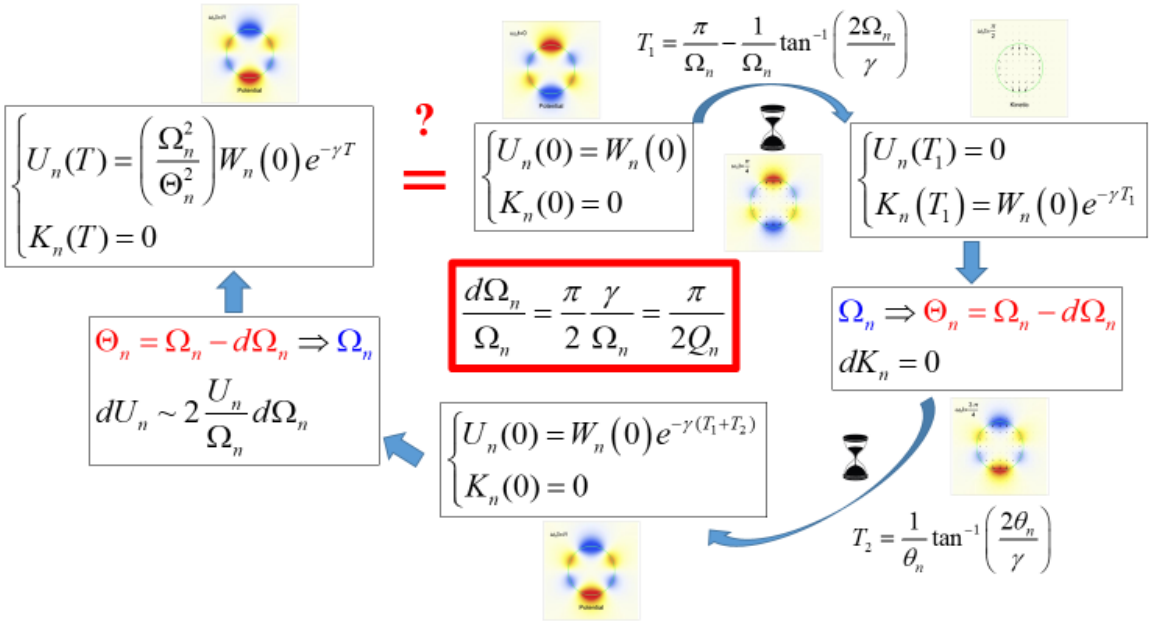

Figure 4.8: Schematic representation of one full-modulation cycle, leading to parametric regeneration of the plasmonic eigenmode

In short, if we have a method of *instantaneously* changing the natural frequency of some mode, we can modulate this natural frequency as discussed in the introduction to Chapter 4.

Furthermore, if this natural frequency modification is timed appropriately, energy can be transferred to the driving mode. In the case of our nanoparticles, the natural frequency must be parametrically increased when the potential energy of the total system is *maximum* and restored to the original value when the potential energy is *zero*. Since the two interactions are π out of phase, we can see in Figure 4.5 that the kinetic energy peaks twice in a 2π cycle, thus, the natural frequency modulation must be applied at twice the desired mode's frequency. Ergo, given a tunable background pump, this mechanism could access resonance modes of arbitrarily high order.

Unlike any other schemes, the presented method relies on a spatially uniform pump field employed to modulate the permittivity of the background material. The analysis for a spherical particle has been presented and the threshold conditions for plasmonic mode amplification have been derived. The presented method could pave the way to a variety of nanoscale nonlinear optical applications of high order plasmonic resonances, including near-field spectroscopy and sensing.

Chapter 5. Conclusions and Future Work

As it currently stands, plasmonics are an area of great interest for the development of next generation wavelength scale devices [35]–[38]. Two novel mechanisms for the delivery of energy to these plasmonic modes have been presented. Both these architectures were rigorously analyzed so as to extract some viable means of control over the plasmonic phenomenon.

When dealing with plasmonic devices on the order of a wavelength, the tolerances for engineering are slim. Through the use of TCOs in a MOS capacitor-like architectures we can relax these tolerances through doping and bias modifications. We've shown that the tunability of the material index is highly flexible in such a device and that guidance is highly localized as long as one stays near, but does not actually reach, a resonance condition. However, to implement such a device as a switching electroabsorbtion modulator, the details of the temporal dynamics of the accumulation layer must be fleshed out. The modulation bandwidth and optical losses of such a device would be strongly dependent on the time dynamics of the switching operation. In our analysis, the accumulation layer charges were considered to be at rest. A unit-step bias function (the prototypical switching operation) would induce a non-linear capacitance function in time as the free charges move across the device into the accumulation layer. In future work, this delay must be analytically understood to enable the use of the ASP as a carrier signal. Additionally, other engineering parameters must be considered, like insertion loss for a device of some finite length and determining optimal dimensions for a such a device.

The second mechanism, termed Plasmonic Parametric Resonance, could have a wide range of applications. Unlike localized plasmonic resonances, parametric resonances phase lock; incoherent oscillations die down while the coherent one grows. This relaxes the excitation

requirements and would potentially allow the PPR to be used as a signal agnostic optical limiter. It's ability to access normally sub radiant modes could also be exploited in some localized sensing applications by amplifying these modes should the appropriate excitation be present. Finally, since these resonance states are highly localized, novel non-linear interactions may be observed at the nano-scale.

Although the PPR concept and theory has been introduced, this analysis is by no means exhaustive. Quality factors achievable with real materials have not been explored and the magnitude of background pump intensity thresholds remains a question. It is speculated that a colloidal suspension of noble metal nano-particles in an organic compound host whose carbon chain has a strong electro-optic effect would be viable, but further analysis is required.

It would be remiss to avoid the fact that, due to analytic complexity, the models provided are cross sectional. That is, three dimensional structures have not been *fully* considered. In the case of the ASP analysis, modulator parameters such as coupling loss from a real fiber would certainly require an understanding of both the longitudinal and transverse cross section of some proposed device. However, a three-dimensional treatment would likely be numerical in nature. In order to maintain the rigor of the presented analytical mathematics, the numerics were chosen only to test and verify the results not as a design tool.

Future work should certainly employ full-wave or multi-physics solvers in three-dimensions to construct physically realizable device models, although it is unclear if results provided by these tools would conform to reality. Without a guiding analytical theory, numerical results may contain artifacts of meshing or sampling and the researcher would be none the wiser. We hope that the model provided here can be used as a basis to extend the treatment into three-dimensions.

In the case of the PPR, another avenue to explore would be the thermal effects of coupling to non-radiative modes. If a PPR optical limiter were designed, some method of cooling may need to be employed. If we consider a nano-particle whose temperature, through the PPR coupling of an absorptive mode, has approached the thermal breakdown temperature of the background suspension as “exhausted”, a regeneration mechanism would be needed to prevent irreversible damage to the system. These thermal considerations would also require a three-dimensional treatment.

While there is a lot of work left to do, in order to bring plasmonics into the state of the art for technological devices the plasmon must be reformed. Engineers must begin to think of the plasmon not as an exotic physical phenomenon but as something that can reliably carry a signal. To that end, this work uncovers some important principles that could lead to new sensor architectures, robust optical absorbers and help bridge the gap between electronics and photonics.

Chapter 6. References

[1] D. Systems, “ITU-T,” 2012.

[2] S. Zhao, L. Lu, L. Zhou, D. Li, Z. Guo, and J. Chen, “16 × 16 silicon Mach–Zehnder interferometer switch actuated with waveguide microheaters,” *Photonics Res.*, vol. 4, no. 5, p. 202, 2016.

[3] R. G. Hunsperger, “Electro-Optic Modulators,” in *Integrated Optics*, Advanced T., Springer, 2002.

[4] M. C. di Piazza and G. Vitale, *Photovoltaic sources: Modeling and emulation*, vol. 53. 2013.

[5] N. W. Ashcroft and . Mermin, N. D, *Solid State Physics*, vol. 2. 1976.

[6] R. W. Boyd 1948-, *Nonlinear optics*, 2nd ed.. San Diego, CA: San Diego, CA : Academic Press, 2003.

[7] C. Kittel, *Introduction to Solid State Physics 8th Edition*. Wiley, 2005.

[8] H. (Heinz) Raether 1909-, “Surface plasmons on smooth and rough surfaces and on gratings.” Berlin , Berlin , 1988.

[9] S. A. Maier, *Plasmonics : fundamentals and applications*. New York: New York : Springer, 2007.

[10] J. P. Colinge, *Physics of Semiconductor Devices*. Springer.

[11] A. Yariv, “Optical waves in crystals : propagation and control of laser radiation.” New York : Wiley, New York, 1983.

[12] J. Leuthold, W. Freude, C. Koos, A. Melikyan, and N. Lindenmann, “A surface plasmon polariton absorption modulator,” *Int. Conf. Transparent Opt. Networks*, vol. 19, no. 9, pp. 8855–8869, 2011.

[13] G. V. Naik, V. M. Shalaev, and A. Boltasseva, “Alternative plasmonic materials: Beyond gold and silver,” *Adv. Mater.*, vol. 25, no. 24, pp. 3264–3294, 2013.

[14] E. Feigenbaum, K. Diest, and H. A. Atwater, “Unity-order index change in transparent conducting oxides at visible frequencies,” *Nano Lett.*, vol. 10, no. 6, pp. 2111–2116, 2010.

[15] J. J. Burke, G. I. Stegeman, and T. Tamir, “Surface-polariton-like waves guided by thin, lossy metal films,” *Phys. Rev. B*, vol. 33, no. 8, pp. 5186–5201, 1986.

[16] V. J. Sorger, N. D. Lanzillotti-Kimura, R. M. Ma, and X. Zhang, “Ultra-compact silicon nanophotonic modulator with broadband response,” *Nanophotonics*, vol. 1, no. 1, pp. 17–22, 2012.

[17] C. Ye, S. Khan, Z. R. Li, E. Simsek, and V. J. Sorger, “λ-Size ito and graphene-based electro-optic modulators on soi,” *IEEE J. Sel. Top. Quantum Electron.*, vol. 20, no. 4, pp. 40–49, 2014.

[18] A. Salandrino and E. A. Ramos, “Accumulation layer surface plasmons,” in *SPIE Metamaterials, Metadevices, and Metasystems*, 2018, no. September, p. 59.

[19] S. Fardad, E. A. Ramos, and A. Salandrino, “Accumulation-layer surface plasmons in transparent conductive oxides,” *Opt. Lett.*, vol. 42, no. 10, pp. 2038–2041, 2017.

[20] N. Engheta, A. Alu, M. G. Silveirinha, A. Salandrino, and Jingjing Li, “DNG, SNG, ENZ and MNZ Metamaterials and Their Potential Applications,” pp. 258–261, 2006.

[21] A. P. Vasudev, J.-H. Kang, J. Park, X. Liu, and M. L. Brongersma, “Electro-optical modulation of a silicon waveguide with an ‘epsilon-near-zero’ material,” *Opt. Express*, vol. 21, no. 22, p. 26387, 2013.

[22] J. C. Butcher, “Runge-Kutta Mtehods,” in *Numeical Methods for Ordinary Differential Equations*, Wiley, 2008, pp. 137–316.

[23] H. Keller, *Numerical Solution of Two Point Boundary Value Problems*. Society for Industrial and Applied Mathematics, 1976.

[24] C. Bender and S. Orszag, *Advanced Mathematical Methods for Scientists and Engineers*. Springer, 2013.

[25] L. Hopf, *Introduction to the Differential Equations of Physics*. Dover Publications, 1948.

[26] W. Magnus 1907-1990, “Hill’s equation.” New York, Interscience Publishers, New York, 1966.

[27] N. W. (Norman W. McLachlan 1888-, “Theory and application of Mathieu functions.” Oxford, Clarendon Press, Oxford, 1947.

[28] A. Salandrino and E. A. Ramos, “High order plasmonic resonances in time-varying media,” *SPIE Metamaterials, Metadevices, Metasystems*, vol. 1034304, no. August 2017, p. 3, 2017.

[29] A. Salandrino, “Plasmonic Parametric Resonance,” *Phys. Rev. B*, 2018.

[30] P. C. Waterman, “Matrix Formulation of Electromagnetic Scattering,” *Proc. IEEE*, vol. 53, no. 8, pp. 805–812, 1965.

[31] C. F. Bohren 1940-, “Absorption and scattering of light by small particles.” New York : Wiley, New York, 1983.

[32] M. Abramowitz 1915-1958 and I. A. Stegun, “Handbook of mathematical functions with formulas, graphs, and mathematical tables.” New York : Wiley, New York, 1972.

[33] B. U. Felderhof and R. B. Jones, “Addition theorems for spherical wave solutions of the vector Helmholtz equation,” *J. Math. Phys.*, vol. 28, no. 4, pp. 836–839, 1987.

[34] G. Arfken and J. E. Romain, “Mathematical Methods for Physicists,” *Phys. Today*, vol. 20, no. 5, p. 79, 1967.

[35] W. Cai, J. S. White, and M. L. Brongersma, “Power-Efficient Electrooptic Plasmonic Modulators,” *Nano Lett.*, vol. 9, no. 12, pp. 4403–4411, 2009.

[36] S. Das, A. Salandrino, J. Z. Wu, and R. Hui, “Near-infrared electro-optic modulator based on plasmonic graphene,” *Opt. Lett.*, vol. 40, no. 7, p. 1516, 2015.

[37] S. Das, I. Kim, J. Rho, R. Hui, and A. Salandrino, “Nanophotonic modal dichroism: mode-multiplexed modulators,” *arXiv.org*, vol. 41, no. 18, 2017.

[38] A. V Krasavin and A. V Zayats, “Electro-optic switching element for dielectric-loaded surface plasmon polariton waveguides,” *Appl. Phys. Lett.*, vol. 97, no. 4, 2010.